

1 **A Comprehensive Observational Based Multiphase Chemical Model**  
2 **Analysis of the Sulfur Dioxide Oxidations in both Summer and**  
3 **Winter**

4

5 *Huan Song<sup>1</sup>, Keding Lu<sup>1\*</sup>, Can Ye<sup>1</sup>, Huabin Dong<sup>1</sup>, Shule Li<sup>1</sup>, Shiyi Chen<sup>1</sup>, Zhijun Wu<sup>1</sup>, Mei Zheng<sup>1</sup>, Limin*  
6 *Zeng<sup>1</sup>, Min Hu<sup>1</sup> & Yuanhang Zhang<sup>1</sup>*

7 State Key Joint Laboratory of Environmental Simulation and Pollution Control, College of Environmental  
8 Sciences and Engineering, Peking University, Beijing, China

9 \*Correspondence to: Keding Lu; ORCID ID: 12465

10

## 11 **Abstract**

12 Sulfate is one of the main components of the haze fine particles and the formation mechanism remains  
13 controversial. Lacking of detailed and comprehensive field data hinders the accurate evaluation of relative  
14 roles of prevailing sulfate formation pathways. Here, we analysed the sulfate production rates using a  
15 state-of-art multiphase model constrained to the observed concentrations of transition metal, nitrogen  
16 dioxide, ozone, hydrogen peroxide, and other important parameters in winter and summer in the North  
17 China Plain. Our results showed that aqueous TMI-catalysed oxidation was the most important pathway  
18 followed by the surface oxidation of Mn in both winter and summer, while the hydroxyl and criegee  
19 radicals oxidations contribute significantly in summer. In addition, we also modelled the published cases  
20 for the fog and cloud conditions. It is found that nitrogen dioxide oxidation is the dominant pathway for  
21 the fog in a higher pH range while hydroperoxide and ozone oxidations dominated for the cloud.

22

## 23 **Introduction**

24 Secondary sulfate aerosol is an important component of fine particles in severe haze periods (Zheng et al.,  
25 2015; Huang et al., 2014b; Guo et al., 2014), which adversely affect the environmental quality and human  
26 health (Lippmann and Thurston, 1996; Fang et al., 2017; Shang et al., 2020). Traditional atmospheric  
27 models evaluate secondary sulfate formation via the gas-phase oxidation of sulfur dioxide (SO<sub>2</sub>) and a  
28 series of multiphase oxidation of dissolved SO<sub>2</sub> in cloud water. During haze events, multiphase oxidation  
29 of dissolved SO<sub>2</sub> is more important than SO<sub>2</sub> directly oxidized by gas-phase radicals (Atkinson et al.,  
30 2004; Barth et al., 2002) because of the significantly reduced ultraviolet (UV) radiation intensity due to  
31 the aerosol dimming effect. Gas-phase reactions, especially those favouring multiphase chemistry, cannot  
32 capture the high concentrations of sulfate aerosols during haze events. Moreover, rapid sulfate production  
33 is observed during cloud-free conditions indicating that aerosol multiphase oxidation may be important  
34 during haze periods (Moch et al., 2018). These effects cause a major gap between the measured sulfate  
35 concentrations under weak UV radiation and the concentrations calculated using traditional atmospheric

36 models.

37 Assessing the mechanism of multiphase secondary sulfate formation during haze periods helps evaluate  
38 the effect of multiphase oxidation. While the gas-phase oxidation rate of SO<sub>2</sub> and OH is well constrained,  
39 there are many uncertainties in the quantification of the relative contribution of each multiphase SO<sub>2</sub>  
40 oxidation pathway during haze periods. Multiphase oxidation pathways of dissolved SO<sub>2</sub> (Seinfeld and  
41 Pandis, 2016; Liu et al., 2020a; Zhu et al., 2020a; Seigneur and Saxena, 1988; Li et al., 2020b) include  
42 oxidation by (1) hydrogen peroxide (H<sub>2</sub>O<sub>2</sub>); (2) ozone (O<sub>3</sub>); (3) transition metal ions [TMI, i.e., Fe (III)  
43 and Mn (II)] catalysed oxidation pathway (aqTMI)]; and (4) Mn-catalysed oxidation of SO<sub>2</sub> on aerosol  
44 surfaces pathway (Mn-surface) (Wang et al., 2021). Some studies (Cheng et al., 2016; Wang et al., 2016;  
45 Xue et al., 2016; Li et al., 2018) also suggested that nitrogen oxides may play a crucial role in the  
46 explosive growth of sulfate formation during severe haze days in Beijing because of the high pH near a  
47 neutral system, by facilitating the catalysis of mineral dust (Liu et al., 2012; Zhao et al., 2018) or the  
48 photolysis of nitrous acid (Zheng et al., 2020). However, the average pH during Beijing haze periods is  
49 approximately 4.2 (Liu et al., 2017), and a high level of NH<sub>3</sub> does not increase the aerosol pH sufficiently  
50 to yield NO<sub>2</sub>-dominated sulfate formation (Guo et al., 2017). Other studies (Ye et al., 2018; Liu et al.,  
51 2020b) emphasized the importance of H<sub>2</sub>O<sub>2</sub> oxidation to sulfate formation due to the underestimation of  
52 H<sub>2</sub>O<sub>2</sub> concentrations during haze episodes in previous studies or the influence of high ionic strength (*I<sub>s</sub>*) of  
53 aerosol solutions on the H<sub>2</sub>O<sub>2</sub> oxidation rate, which implies that oxidant concentrations for SO<sub>2</sub> oxidation  
54 constrained to the observed values from field measurements are required. Previous study (Wang et al.,  
55 2020) showed that photosensitization is a new pathway for atmospheric sulfate formation and requires  
56 further verification. According to previous studies of the GEOS-Chem model and including the  
57 measurements of oxygen isotopes ( $\Delta^{17}\text{O}$  (SO<sub>4</sub><sup>2-</sup>)) (He et al., 2018; Shao et al., 2019; Li et al., 2020a; Yue  
58 et al., 2020), several studies showed that aqTMI was important during some haze periods. Overall, the  
59 formation mechanisms of the missing sulfate sources remain unclear and controversial.

60 Sulfate formation is a complex multiphase physicochemical reaction process, in which parameters have  
61 multiple interrelationships. The previous studies have mostly selected typical conditions with fixed

62 parameters for numerical calculations, ignoring the fact that sulfate formation is a complex dynamic  
63 process. A comprehensive and explicit evaluation of the sulfate generation process requires real-time  
64 feedback and explicit constraints of observational data. Therefore, it is crucial to apply constrained  
65 parameters from field campaigns in the calculations. Moreover, as proposed in previous studies (Liu et  
66 al., 2020b; Cheng et al., 2016), due to the lower water content in aerosol particles than in cloud water, the  
67 non-ideality effects of aerosol solutions should be carefully considered.

68 In this study, we modelled the concentrations of the main reagents of sulphate formation reactions using a  
69 state-of-art Peking-University-Multiple-phAse Reaction Kinetic Model (PKU-MARK) based on the data  
70 measured in two field campaigns conducted in the winter and summer in the North China Plain (NCP)  
71 where several particle pollutions happened. The non-ideality of aerosol solutions was considered in the  
72 calculation of both gas solubility and aqueous-phase reaction rates. Chemical regimes in the aerosol  
73 particle bulk phase were analysed to understand the role of gas-phase radical precursors, particle TMIs,  
74 aerosol surface concentrations and the aerosol liquid water content (ALWC) on the aqueous reactant  
75 levels and the sulfate formation rate. All particle concentrations reported are fine particle matters  
76 particulate matter with aerodynamic diameter of 2.5  $\mu\text{m}$  or less ( $\text{PM}_{2.5}$ ).

77 The overall goal of this work is to evaluate the contribution of different secondary sulfate formation  
78 pathways under actual field measurement conditions in the NCP. Effects of non-ideality of condensed  
79 particle phase and the solubility of gas-phase reactants on the reactions enable the comparisons with  
80 parameters previously obtained in model calculations. In addition, episodes at different pollution levels in  
81 the winter and summer campaigns were selected to evaluate the contribution of prevailing sulfate  
82 formation pathways proposed in previous studies. As a study evaluating the contribution of different  
83 sulfate formation pathways during field campaign observations, this work provides an improved  
84 understanding of atmospheric sulfate formation at different pollution levels in the NCP.

85

86

## 87 **2 Results**

### 88 **2.1 Overview of the field observations**

89 Table 1 shows the key meteorological parameters, trace gases concentrations, calculated ALWC, ionic  
90 strength, pH and sulfate formation rates under different pollution conditions in PKU-17 and WD-14  
91 comprehensive field campaigns. Sampling location and experimental methods used in these two  
92 campaigns are summarized in the Method part. The pollution degree is classified according to the mass  
93 concentration of  $PM_{2.5}$ . The clean condition means  $PM_{2.5}$  smaller than  $35 \mu\text{g}/\text{m}^3$ , the slightly polluted  
94 condition is  $35\text{-}75 \mu\text{g}/\text{m}^3$ , the polluted condition is  $75\text{-}150 \mu\text{g}/\text{m}^3$  and highly polluted is larger than  $150$   
95  $\mu\text{g}/\text{m}^3$ . Sulfate formation rates were modelled by the Multiple-phAse Reaction Kinetic Model (PKU-  
96 MARK) (mentioned in Method) with constrained parameters. The effects of aerosol non-ideality were  
97 considered in the size-segregated model. Data points with relative humidity (RH) smaller than 20% and  
98 AWLC smaller than  $1 \mu\text{g}/\text{m}^3$  were abandoned to improve the accuracy of the results.

99 Transition metals concentrations including Fe and Mn increased with PM mass (as shown in Fig.1).  
100 Photochemical oxidants including  $\text{H}_2\text{O}_2$  and  $\text{O}_3$  exhibited a decreasing trend with the increase of PM mass  
101 because of the significantly reduced solar ultraviolet (UV) radiation intensity due to the aerosol dimming  
102 effect. Some studies reported high  $\text{H}_2\text{O}_2$  concentrations during haze episodes (Ye et al., 2018), whereas in  
103 PKU-17 field campaign, the average concentration of  $\text{H}_2\text{O}_2$  was only  $20.9\pm 22.8$  pptV in highly polluted  
104 conditions. Higher sulfate concentration was observed in the high range of RH and ALWC indicating  
105 their enhancement effects on the sulfate formation. We also picked four haze periods in PKU-17  
106 observation, the time series of these key parameters are provided in Supplementary Information (SI) **Fig.**  
107 **S4**.

108 Aerosol pH values were calculated using the ISORROPIA-II model. The calculated particle pH values as  
109 shown in the **Table 1** are in good agreement with the values reported in other studies (Guo et al., 2017;  
110 Weber et al., 2016). The lower pH in the range of 4.0–5.5 is beneficial to sulfate formation via aqTMI.  
111 Aerosol liquid water is another key component, higher loading of aerosol liquid water is more conducive

112 to the occurrence of multiphase reactions. The ALWC in the PKU-17 and WD-14 campaigns was  
113 calculated via the ISORROPIA II model with input concentrations of aerosol inorganic components (see  
114 **Method M.3**). Aerosol liquid water did not freeze at winter temperatures below 273 K in the PKU field  
115 campaign because of the salt induced freezing point depression (Koop et al., 2000). Wind speeds during  
116 these haze events were persistently low (0.3–1.5 m/s), indicating the minor contribution of regional  
117 transport to sulfate production.

118 Aqueous TMI concentration level is crucial in the evaluation of secondary sulfate formation in real  
119 atmospheric conditions. Atmospheric anthropogenic sources of transition metals such as iron (Fe) are  
120 crust related and the peak concentration of Fe in Beijing is correlated to the vehicle driving in traffic rush  
121 hours. Copper (Cu), and manganese (Mn) are mainly from non-exhaust emissions of vehicles, fossil fuel  
122 combustion or metallurgy (Alexander et al., 2009; Duan et al., 2012; Zhao et al., 2021). Concentrations of  
123 transition metals are highly variable, ranging from  $<0.1 \text{ ng m}^{-3}$  to  $>1000 \text{ ng m}^{-3}$  globally (Alexander et  
124 al., 2009). Fe solubility in atmospheric aerosols has been reported to range from 0.1% to 80% (Ito et al.,  
125 2019; Hsu et al., 2010; Heal et al., 2005; Shi et al., 2012; Mahowald et al., 2005), and elevated levels of  
126 Fe solubility have been observed in aerosols dominated by combustion sources. The average fractional Fe  
127 solubility in areas away from dust source regions is typically between 5 and 25% (Baker and Jickells,  
128 2006; Baker et al., 2006; Hsu et al., 2010). A recent study reported the average Fe solubility as 2.7–5.0%  
129 in Chinese cities, and more than 65% of nano-sized Fe-containing particles were internally mixed with  
130 sulfates and nitrates (Zhu et al., 2020b). The solubility of Mn tends to be higher than that of Fe (Baker et  
131 al., 2006), which is 22–57% in urban aerosol particles (Huang et al., 2014c). In this study, we chose the  
132 solubility of total Fe as 5% and total Mn solubility as 50% assuming that aerosol particles are internally  
133 mixed. In Beijing, high concentrations of Fe, Cu, and Mn were observed (**Table S9**). Concentrations of  
134 transition metals are strongly correlated during these haze periods; thus, we propose a fixed ratio of  
135 Fe/Mn to account for the lack of Mn data in PKU-17 and WD-14 field campaigns (**SI Text S2**).

136 Aerosol trace metal speciation and water solubility are affected by factors such as photochemistry, aerosol  
137 pH, and aerosol particle size (Baker and Jickells, 2006; Oakes et al., 2010). Soluble iron in aerosol water  
138 exists as Fe (II) and Fe (III), with a series of redox recycling between the two species and other ions.  
139 Partitioning between Fe (II) and Fe (III) varies diurnally with the highest fraction of Fe (II) found during  
140 the day because of the photochemical reactions reducing Fe (III) to Fe (II). Photolysis reactions of iron  
141 hydroxides and organic complexes were documented as the most important source of Fe (II) in cloud and  
142 fog water. Oxalic acid and its deprotonated form, oxalate, have strong coordination ability with Fe and  
143 form Fe-oxalate complexes, which have higher photochemical activity than Fe hydroxide. All these  
144 mechanisms are included in the PKU-MARK model. Diurnal trends of sulfate formation were observed  
145 during haze periods indicating the diurnal distribution of different states of iron. Redox cycling of other  
146 TMIs such as Cu and Mn are also considered in the PKU-MARK model. Averaged percentage of soluble  
147 Fe (III) and Mn (II) was 0.79% and 19.83% in winter polluted conditions and 2.57% and 52.15% in  
148 summer polluted conditions. The main reason for the difference between winter and summer metal  
149 solubility is that summer aerosols have higher water content and lower ionic strength, which is conducive  
150 to the dissolution of Fe and Mn. The solubility range is in good agreement with the values reported in  
151 previous observations (Ito et al., 2019; Hsu et al., 2010).

152 The influence of aerosol ionic strength on aqTMI reaction rates was considered carefully in the study.  
153 Higher ALWC is typically accompanied by lower ionic strength, which increases the activity of TMI. The  
154 relationship (Liu et al., 2020b) between the rate coefficients of the TMI pathway and ionic strength is  
155 displayed in **Fig. S1**. The sulfate formation rate decreased by 424.82 times when ionic strength was 45 M  
156 compared to the dilute solution with ionic strength of 0 M. Despite considering the effect of the activity  
157 coefficient on the reaction rate of aqTMI, the contribution of the aqTMI was still dominant during haze  
158 periods indicating that the dominance of aqTMI can be a widespread phenomenon, as recommended in  
159 previous studies (He et al., 2018; Shao et al., 2019; Li et al., 2020a; Yue et al., 2020).

## 160 **2.2 Analysis of sulfate formation rate in different pollution conditions**

161 **Fig. 1 (a) and (b)** display the 3-h averaged sulfate formation rates in the PKU-17 and WD-14 during haze  
162 periods. Contributions of the gas-phase radical oxidants were much higher during summer time. To fully  
163 explain the relative contributions to sulfate formation from different pathways, the stabilized criegee  
164 intermediates (SCIs) oxidant was also considered in the calculations. Based on the previous report  
165 (Sarwar, 2013), the inclusion of the SCIs oxidation pathway further enhances sulfate production. We  
166 modified the Regional Atmospheric Chemistry Mechanism (RACM2) (Goliff et al., 2013; Goliff and  
167 Stockwell, 2008) to represent three explicit SCIs and their subsequent reactions (Welz et al., 2012) with  
168 SO<sub>2</sub>, NO<sub>2</sub>, aldehydes, ketones, water monomer, and water dimer and calculated the contribution of this  
169 pathway in two field campaigns.

170 The contribution of aqTMI increased rapidly with the aggravated pollution. High concentrations of  
171 transition metals observed in Beijing facilitated the dissolution of Fe, Cu, and Mn. The relationship of  
172 ionic strength and aqTMI rate constant is illustrated in **SI Fig. S1** and **Table S2** (Liu et al., 2020b).  $\alpha\text{Fe(III)}$   
173 (III) is defined as the product of the Fe (III) activity coefficient, concentration, molecular weight (56) and  
174 aerosol liquid water content. Compared to the total Fe concentration, it is more effective to evaluate the  
175 impact of  $\alpha\text{Fe(III)}$  on sulfate formation. The relationship between  $\alpha\text{Fe(III)}$  and SOR  
176 ( $\equiv n(\text{SO}_2)/n(\text{SO}_2+\text{SO}_4^{2-})$ , defined as the ratio of mole concentration of SO<sub>2</sub> with the sum of SO<sub>2</sub> and SO<sub>4</sub><sup>2-</sup>  
177 mole concentrations) in PKU-17 winter field campaign was shown in **SI Figure S5**. Because of the  
178 inhibition of the effects of high ionic strength on the rate constant of aqTMI, a high volume of aerosol  
179 water during the haze event increased the TMI activity coefficient benefiting sulfate formation. Obvious  
180 correlations between  $\alpha\text{Fe(III)}$  and sulfate concentration shown in **Fig. 1 (c) and (d)** were observed in the  
181 haze periods both in summer ( $R^2=0.63$ ) and winter ( $R^2=0.71$ ) and the correlation is consistent with the  
182 important contributions from aqTMI pathway to the sulfate formation. Affected by the higher boundary  
183 layer height and higher gas phase radical concentration in summer, the correlation between sulfate  
184 oxidant ratio SOR and PM mass in summer is not as significant as that in winter. In summer, as illustrated  
185 in **Fig. S6**, there was still an obvious positive dependence between SOR and RH and ALWC, whereas a



186 negative correlation was found between SOR and odd-oxygen ( $[Ox] \equiv [O_3] + [NO_2]$ ). As shown in **Fig. 1 (e)**  
187 **and (f)**, the sulfate formation through gaseous reaction was more important in summer than in winter,  
188 mainly provided by gas phase radicals (OH and SCIs). In WD-14 field campaign, heterogeneous aqTMI  
189 pathways were still dominant in the secondary sulfate formation.

### 190 **2.3 Dependence of the Secondary sulfate formation rates on aerosol pH and** 191 **water content**

192 Aerosol pH and ALWC were calculated using the ISORROPIA-II model (Method M3). Because of the  
193 high sensitivity of sulfate formation to pH, the lower range of aerosol pH during these two campaigns  
194 made the aqTMI the most important one. The effects of high aerosol ionic strength on the dissolution  
195 equilibrium and reaction rates were considered in calculations (Liu et al., 2020b) (**SI Table S2 to S4**).  
196 Due to the low  $H_2O_2$  concentration ( $\sim 0.023$  ppbV) and low ALWC observed in the PKU-17 field  
197 campaign, the average contribution of  $H_2O_2$  in haze periods ( $PM_{2.5} > 75 \mu g/m^3$ ) was about  $0.11 \pm 0.15$   
198  $\mu g/m^3/h$ . Higher gas-phase  $H_2O_2$  concentration may further increase the contribution of this pathway to  
199 sulfate formation. Based on a recent report (Ye et al., 2018), higher gas-phase  $H_2O_2$  concentrations were  
200 observed in the NCP during different haze events, including severe haze episodes in suburban areas. At  
201  $0.1$  ppbV  $H_2O_2$  (about five times higher than the observed  $H_2O_2$  concentration), the calculated sulfate  
202 formation rate was  $0.52 \pm 0.76 \mu g/m^3/h$  in haze periods with great uncertainty and still lower than the  
203 contribution of the TMI pathway ( $1.17 \pm 1.48 \mu g/m^3/h$ ).

204 Due to the potential interaction between various factors in the atmosphere, fixing certain parameters and  
205 changing only the pH to obtain the sulfate production rate may cause errors. With the development of  
206 haze, concentrations of  $O_3$  and OH radicals decrease due to reduced UV radiation caused by the aerosol  
207 dimming effect. Despite its minor contribution to sulfate production in winter, the increase in the ozone  
208 oxidation rate with pH was slower under actual conditions. Contributions of gas-phase radicals also  
209 showed a weak downward trend in the summer campaign (**Fig. 2 (c)**). The bias between calculated and  
210 observed values indicated a dynamic balance of atmospheric oxidation in the gas phase and aerosol phase.

211 If we arbitrarily use the average values during haze periods and only changed the pH of the aerosols as in  
 212 previous studies, the obtained sulfate production rate will deviate from the observed values. Actual  
 213 ambient sulfate formation rates calculated using the measured values in polluted periods in two field  
 214 campaigns are illustrated in **Fig. 2 (a) and (c)**. Average values except for pH during the haze periods were  
 215 used to calculate the sulfate formation rates as shown in **Fig. 2 (b) and (d)**. The peak of the H<sub>2</sub>O<sub>2</sub> line in  
 216 the figure is caused by the change in the water content and ionic strength. In the pH range of 4.0–6.0, the  
 217 calculated ALWC was in the highest range, increasing the contribution of H<sub>2</sub>O<sub>2</sub> proportionally as  
 218 calculated using **equation (1)**.

219 Aerosol water content is another key factor that influences the contribution of different pathway to sulfate  
 220 formation. In the calculation, we changed the unit of sulfate formation rate from  $\mu\text{g}/\text{m}^3_{\text{air}}$  to  $\text{mol}/\text{s} \cdot \text{L}_{\text{water}}$   
 221 and the sulfate formation rate can be calculated via the following equation with the modeled

222  $\frac{dS(VI)}{dt}$  ( $M/s$ ):

$$223 \quad \frac{dS(VI)}{dt} (\mu\text{g m}^{-3} \cdot \text{h}^{-1}) = 0.01 \times 3600 (\text{s h}^{-1}) \cdot 96 \text{ g mol}^{-1} \cdot \frac{dS(VI)}{dt} (\text{M s}^{-1}) \cdot \frac{ALWC}{\rho_{\text{water}}} \quad (1)$$

224 where ALWC is in units of  $\mu\text{g m}^{-3}$  and  $\rho_{\text{water}}$  is the water density in  $\text{kg L}^{-1}$ . At high ionic strength, this  
 225 expression is more accurate than the equivalent expression with the unit of  $\text{M s}^{-1}$ . The equilibrium amount  
 226 of H<sub>2</sub>O<sub>2</sub>, O<sub>3</sub>, and NO<sub>2</sub> in units of  $\mu\text{g}/\text{m}^3_{\text{air}}$  is controlled by the amount of ALW, ie there is equilibrium  
 227 between gas and particle water for these oxidants formed in the gas phase. And total amount of metal  
 228 elements, Fe, Cu or Mn is not dependent on aerosol water content. Aerosol water content does not affect  
 229 TMI levels in solution by affecting the solubility of the overall metal form of the specific species (**Fig.3**  
 230 shows insensitivity of pH to ALWC, which has been pointed out in other papers (Wong et al., 2020). The  
 231 reaction kinetics and rate constants summarized in **Table S2** suggest that there is a proportional  
 232 relationship between ALWC and sulfate formation pathways except aqTMI. One reason for the lower  
 233 sulfate formation rate observed in the PKU-17 ( $1\text{--}3 \mu\text{g m}^{-3} \text{ h}^{-1}$ ) is that the ALWC values were lower than  
 234 those assumed in previous studies ( $\text{ALWC} = 300 \mu\text{g m}^{-3}$ ). This deviation from the ALWC significantly

235 reduces the contribution of several other pathways, but not the contribution of transition metals to sulfate  
236 formation.

237 Due to the obvious heterogeneous reaction's contribution to sulfate formation in winter, we evaluated the  
238 influence of ALWC on sulfate formation pathways in winter. TMI relevant pathways including aqTMI  
239 and Mn-surface pathway were dominate in all range of ALWC as illustrated in **Fig.3**. In PKU-17 field  
240 campaign, with the increasing of ALWC from 1 to 150  $\mu\text{g}/\text{m}^3$ , the ratio of Mn-surface/aqTMI  
241 continuously decreased mainly because of the decreasing particle specific surface areas. Mn-surface  
242 contributed most in lower ALWC range where particle specific surface area was high and provide more  
243 reaction positions. Aqueous transition metal ions mole concentration decreasing with the aerosol  
244 hygroscopic growth indicating a "dilution effect" as shown in **Fig. S7** with the aerosol hygroscopic  
245 growth, the increasing of transition metal total mass in air is slower than water mass in PKU-17. The ratio  
246 of Fe total mass ( $\text{Fe}_t$ )/ALWC decreasing with  $\text{PM}_{2.5}$  mass. Previous global scale observations (Sholkovitz  
247 et al., 2012) of  $\sim 1100$  samples also showed the hyperbolic trends of Fe solubility with total Fe mass.  
248 Higher activity coefficients and lower aqueous TMI concentration led to the emergence of "high  
249 platform" of the aqTMI pathways contribution to sulfate formation in the range of 50-150  $\mu\text{g}/\text{m}^3$  ALWC  
250 (ie, higher effective aqueous TMI in this range). While ALWC exceeding 150  $\mu\text{g}/\text{m}^3$  in winter, the  
251 increase of activity coefficients could not promote the rate of aqTMI. Due to the slight increase of aerosol  
252 pH and the dilution effect of aerosol hygroscopic growth on TMI when ALWC exceeding 150  $\mu\text{g}/\text{m}^3$  as  
253 discussed above, the importance of aqTMI and Mn-surface contributions were lowered. At this time, the  
254 contributions of external oxidizing substances pathways such as  $\text{H}_2\text{O}_2$ ,  $\text{NO}_2$  or  $\text{O}_3$  may rise in the proper  
255 pH range as illustrated in **Fig.4**. In winter fog or cloud conditions with higher water content, the  
256 contribution from TMI may decrease a lot for their low solubility and concentrations.

257 The same analysis also used in the summer WD-14 field campaign (as shown in **SI Fig.S8**). "The dilution  
258 effect" occurred more dramatically in summer compared to that in winter because of a higher RH and  
259 higher percentage of water in the aerosol. In this situation, the contribution of aqTMI or Mn-surface was  
260 inhibited due to the low soluble TMI concentrations. Considering the positive relationships of SOR and

261 RH in summer WD-14 field campaign, aqueous and surface sulfate formation contributions mentioned in  
262 the study could not explain the missing source of secondary sulfate. Because of the low pH range  
263 observed in WD-14 field campaign, the contributions from  $\text{H}_2\text{O}_2$ ,  $\text{NO}_2$ ,  $\text{O}_3$  or  $\text{NO}_3^-$  photolysis were  
264 negligible. The missing contribution may mainly come from other pathways such as photosensitizing  
265 molecules (Wang et al., 2020) under stronger UV in summer or contributions from hydroxy methane  
266 sulfonate (Moch et al., 2018; Ma et al., 2020) which need further studies.

267

## 268 **Discussion and Conclusion**

269 We evaluated the contribution of different pathways to secondary sulfate formation using a state-of-art  
270 size-segregated multiphase model constrained to the observed parameters from two field campaigns in the  
271 North China Plain. In addition, the effects of aerosol solution non-ideality on aqueous-phase reaction rates  
272 as well as dissolution equilibria were considered in the calculations. The results indicated that the  
273 aqueous TMI-catalysed oxidation pathway (aqTMI) was an important contributor to sulfate formation  
274 during haze episodes, which is consistent with the results of the isotope and WRF-CHEM studies (He et  
275 al., 2018; Shao et al., 2019; Li et al., 2020a; Yue et al., 2020).

276 Despite the dominant role of aqTMI in PKU-17 field campaign, contributions from other multiphase  
277 pathways are not negligible. Dominant pathways varied with conditions such as clear or haze periods in  
278 clouds or aerosol water. **Fig. 4** exhibits the contribution of different oxidation pathways to sulfate  
279 formation in aerosol water (under different pollution levels), fog, and clouds to indicate the dominant  
280 factors of sulfate formation under different conditions. In clear periods, gas-phase oxidation of SO<sub>2</sub> by gas  
281 phase radicals (OH and SCIs) happens continuously, contributing 0.01–0.6 μg/m<sup>3</sup>/h to sulfate formation.  
282 At the clean time, sulfate production is mainly limited by relatively low SO<sub>2</sub> concentrations and low  
283 ALWC, which has promotion effects on the multiphase sulfate formation pathways. The average sulfate  
284 formation rate during clear days was 1.30 μg/m<sup>3</sup>/h in winter and 2.13 μg/m<sup>3</sup>/h in summer because of the  
285 generally higher ALWC in summer aerosol and much higher gas phase radical concentrations. Gas-phase  
286 radicals (OH and SCIs) continuously oxidize SO<sub>2</sub> during the haze and clear periods.

287 External oxidizing substances such as NO<sub>2</sub> and O<sub>3</sub> had little contribution to sulfate formation during these  
288 haze periods because of the high aerosol acidity. High pH (near 7) values were observed in these field  
289 campaigns when the contribution of the NO<sub>2</sub> pathway was dominant at some point but not during the  
290 entire pollution process; its proportion was much lower than that of aqTMI. Although the enhancement  
291 factor of H<sub>2</sub>O<sub>2</sub> oxidation was considered based on the measurement of previous study (Liu et al., 2020b),

292 the contribution of H<sub>2</sub>O<sub>2</sub> oxidation was still below 0.5 μg S(VI)/m<sup>3</sup>/h because ALWC was about 10 times  
293 lower than 300 μg m<sup>-3</sup>, which was used in previous studies (Cheng et al., 2016; Liu et al., 2020b).  
294 The sulfate formation rate is limited by the ALWC according to **equation (1)**. Aerosol particles have  
295 lower water content than cloud droplets, which provides larger space for aqueous phase reactions.  
296 Therefore, at the gas-phase SO<sub>2</sub> concentrations of 5–50 ppb, 10–100 times higher water content in fog and  
297 cloud droplets can cause higher sulfate formation rates up to 100 μg m<sup>-3</sup> h<sup>-1</sup> assuming 0.1 g m<sup>-3</sup> water in  
298 clouds (**Fig. 4**). A high H<sub>2</sub>O<sub>2</sub> concentration (1 ppb), which was 50 times higher than that in the PKU field  
299 campaign, was used in the calculation in the Cloud\_5.0 regime (Seinfeld and Pandis, 2016). No obvious  
300 contribution from the NO<sub>2</sub> oxidation pathway was observed in the PKU-17 and WD-14 field campaigns  
301 because of the lower pH range. As proposed in a previous study, the particulate nitrate photolysis can  
302 explain the missing source of sulfate in Beijing haze (Zheng et al., 2020). However, according to the  
303 recent laboratory report (Shi et al., 2021), the nitrate photolysis enhancement factor is no larger than 2 at  
304 all RH ranges. We also included the calculation of nitrate photolysis in this study due to the high loading  
305 of particle nitrate and found that the contribution was rather small (~0.008 μg m<sup>-3</sup> h<sup>-1</sup> in winter haze  
306 periods); thus, we did not include this pathway in the figures.

307 According to our modelled results and the newest study (Wang et al., 2021), Mn surface reactions  
308 contributed a lot to sulfate formation. Except for possible Mn(OH)<sub>x</sub><sup>(3-x)</sup> reacting with SO<sub>2</sub>, Zhang et al.  
309 (2006) proposed that other metal oxides such as Fe<sub>2</sub>O<sub>3</sub> and Al<sub>2</sub>O<sub>3</sub> can also react with SO<sub>2</sub> on the surface  
310 of particles. While as mentioned above, the ratio of contributions from Mn-surface/ aqTMI to produce  
311 sulfate will decrease with aerosol hygroscopic growth owing higher ALWC and lower specific surface  
312 areas (as shown in **Fig.3** panel (b) black dotted line). What's more, the organic coating of aerosol particles  
313 can largely reduce the reactivity of surface heterogeneous reactions (Zelenov et al., 2017; Anttila et al.,  
314 2006; Folkers et al., 2003; Ryder et al., 2015) and may cause the Mn-surface pathway less important.  
315 High mass concentrations of organic aerosol (OA) were observed in Beijing both in winter and summer  
316 (Hu et al., 2016), based on measured result (Yu et al., 2019) from transmission electron microscopy, up to  
317 74 % by a number of non-sea-salt sulfate particles were coated with organic matter (OM). The organic

318 coating can effectively reduce the reactive sites in the surface of particles hence reduce the reaction  
319 probability of SO<sub>2</sub> with surface metal. In the other hand, the widespread presence of aerosol organic  
320 coating can also influence the bulk SO<sub>2</sub> catalysed by aqueous TMI but not only the surface reactions. This  
321 effect is mainly achieved by the change of SO<sub>2</sub> solubility and diffusion coefficient rather than the rates of  
322 catalytic reactions with TMI. Although the solubility of SO<sub>2</sub> in organic solvent changes a lot with the  
323 component of organic (Zhang et al., 2013; Huang et al., 2014a), according to previous studies of SO<sub>2</sub>  
324 uptake coefficient with sea-salt aerosol (Gebel et al., 2000) and secondary organic aerosol (SOA) (Yao et  
325 al., 2019), no obvious uptake coefficient reduction was observed with the organic coating further proving  
326 the minor influence of the organic coating on bulk reaction rates. The catalytic reaction of SO<sub>2</sub> with  
327 aqTMI may less affected by aerosol organic coating compared to SO<sub>2</sub> with Mn-surface. For these reasons,  
328 the surface reaction of SO<sub>2</sub> with Mn and other metals in actual aerosol conditions remain unclear with  
329 high uncertainties and need further evaluation. The relevant calculation results of WD-14 and PKU-17 in  
330 this paper represent the upper limit of Mn-surface contribution. The missing contribution in WD-14  
331 polluted conditions may mainly come from organic photosensitizing molecules such as HULIS (Wang et  
332 al., 2020) under stronger UV in summer or other SOA coupled mechanisms.

333 The results in this paper indicate that sulfate formation has different chemical behaviours in different  
334 conditions. Aqueous TMI-catalysed oxidation was the most important pathway followed by the surface  
335 oxidation of Mn in both winter and summer, while the hydroxyl and criegee radicals oxidations contribute  
336 significantly in summer. Due to the differences in the physical and chemical properties between aerosol  
337 water, fog water and cloud, nitrogen dioxide oxidation is the dominant pathway in higher pH range and  
338 hydroperoxide and ozone oxidations dominated for the cloud. In model studies, the averaged and fixed  
339 values should be used dialectically and carefully in the calculation of sulfate formation rate because of the  
340 mutual restriction between factors such as pH, effective ion activity and concentration, and aerosol water  
341 content. Model evaluation or numerical calculations of secondary pollutants should focus on the  
342 application of actual atmospheric conditions observed in field campaigns with the application of closure  
343 study. Our results highlight the important role of aerosol aqTMI in sulfate formation during haze periods

344 and the monitoring network of aerosol metal is necessary for the studies of secondary sulfate formation.  
345 The aqTMI independent of solar radiation also explains the explosive growth of sulfate production at  
346 night-time, which is frequently observed during haze episodes in the NCP.  
347 Compared to the gas-phase oxidants, the control of anthropogenic emissions of aerosol TMI is conducive  
348 to the reduction of secondary sulfates. The promotion of clean energy strategies aiming at reducing coal  
349 burning and vehicle emissions to improve air quality in North China has reduced not only the primary  
350 emissions of SO<sub>2</sub> but also the anthropogenic emissions of aerosol TMIs (Liu et al., 2018) and thus the  
351 production of secondary sulfate. What' more, China's ecological and environmental protection measures  
352 for tree planting and afforestation are conducive to reducing the generation of dust especially in the spring  
353 can further reducing the quality of metal Fe concentrations in aerosols.  
354 Our findings showed that urban aerosol TMIs contribute to sulfate formation during haze episodes and  
355 play a key role in developing mitigation strategies and public health measures in megacities worldwide,  
356 but the physicochemical processes of transition metals in particles require further research. Dissolved Mn  
357 concentrations in this study were estimated based on previous studies. The solubility of transition metals  
358 in aerosol water varying largely due to several factors including various source emissions, aerosol organic  
359 matter and pH (Paris and Desboeufs, 2013; Wozniak et al., 2015; Tapparo et al., 2020) were not fully  
360 considered in this study. Influences of organic matter and photosensitizing molecules on the solubility of  
361 transition metal and the mechanism of sulfate formation need further research to understand this complex  
362 and dynamic multiphase process from a broader perspective.

363

## 364 **Methods**

### 365 **M. 1 Sampling location and experimental methods**

366 The data from the 2014 Wangdu (WD) and 2017 Peking University (PKU) field campaigns, both  
367 conducted in summer, were used in our analysis. The WD field campaign was carried out from June to  
368 July 2014 at a rural site in Hebei (38.70° N, 115.15° E) characterized by severe photochemical smog



369 pollution (Tan et al., 2017; Song et al., 2020). The 2017 PKU campaign was performed from November  
370 to December 2017 at the campus of Peking University (39.99° N, 116.31° E), which is in the city centre  
371 of Beijing and characterized by strong local anthropogenic emissions from two major roads (Ma et al.,  
372 2019).

373 Observations from both field campaigns include gas-phase measurements of SO<sub>2</sub> and O<sub>3</sub> from commercial  
374 Thermo Scientific monitors and NO<sub>2</sub> detected after conversion through a custom-built photolytic  
375 converter with UV-LED at 395 nm; aerosol number concentration and distribution from a set of  
376 commercial particle instruments containing Nano scanning mobility particle sizer (SMPS) and  
377 aerodynamic particle sizer (APS) to cover the size range of 3 nm to 10 μm. The mass concentration of  
378 PM<sub>2.5</sub> was measured by commercial Ambient Particulate Monitor (TEOM). The In-situ Gas and Aerosol  
379 Compositions monitor (IGAC) (Young et al., 2016), which can collect gases and particles  
380 simultaneously, was used to measure water-soluble ions online with 1-h time resolution. Both gas and  
381 aerosol samples were injected into 10 mL glass syringes, which were connected to an ion chromatograph  
382 (IC) for analysis (30-min time resolution for each sample). The concentrations of eight water soluble  
383 inorganic ions (NH<sub>4</sub><sup>+</sup>, Na<sup>+</sup>, K<sup>+</sup>, Ca<sup>2+</sup>, Mg<sup>2+</sup>, SO<sub>4</sub><sup>2-</sup>, NO<sub>3</sub><sup>-</sup>, and Cl<sup>-</sup>) in fine particles were measured.

384 Transition metal (Fe and Cu) concentrations in PM<sub>2.5</sub> were measured using the Xact 625 Ambient Metal  
385 Monitor. With Xact, ambient air was introduced through a PM<sub>2.5</sub> cyclone inlet at a constant flow rate of  
386 16.7 L min<sup>-1</sup> and collected on the reel-to-reel poly tetrafluoroethylene filter. Then trace elements in  
387 ambient fine particles on the filter were automatically detected using the United States Environmental  
388 Protection Agency (USEPA) standard method via x-ray fluorescence (XRF) analysis (Gao et al., 2016;  
389 Zhang et al., 2019). Ambient temperature and pressure data were measured using commercial  
390 meteorological sensors; selected volatile organic compounds (VOCs) were measured via off-line gas  
391 chromatography–mass spectrometry (GC-MS) in tower measurements using sampling canisters and via  
392 online GC–MS in the surface campaign. The OH and HO<sub>2</sub> concentrations were measured via laser-  
393 induced fluorescence (LIF) with the time resolution of 30 s as described in previous study (Ma et al.,

394 2019). The concentrations of gas-phase peroxides were measured using high-performance liquid  
395 chromatography (HPLC, Agilent 1200, USA) with a time resolution of 21 min.

## 396 **M. 2 Brief overview of the PKU-MARK model**

397 The Multiple-phAse Reaction Kinetic Model (PKU-MARK) was first developed to calculate the  
398 heterogeneous reaction rate of reactive gas molecules (Song et al., 2020). The units of aqueous reagents  
399 are converted to molecules·cm<sup>-3</sup> in the model by a factor  $k_{mi}$ , which combines both gas-phase molecular  
400 diffusion and liquid-phase interface mass transport processes (Schwartz, 1984; Schwartz, 1986) and used  
401 in the calculation for gas–liquid multiphase reactions in many modelling studies (Lelieveld and Crutzen,  
402 1991; Chameides and Stelson, 1992a; Sander, 1999; Hanson et al., 1994; Song et al., 2020). In this study,  
403 the PKU-MARK model was further developed with the correction of ionic strength for all ions and  
404 reactants and applied to a size-segregated system to investigate the influence of aerosol particle size  
405 distribution and ALWC distribution. Eleven bins of aerosol particle diameters and corresponding ALWC  
406 values were applied in the model. With the input of one-hour averaged parameters observed in the field  
407 campaign, the PKU-MARK model produced the state-state concentrations of aqueous reactants including  
408 reactive oxygen species (H<sub>2</sub>O<sub>2</sub>, O<sub>3</sub>, OH, HO<sub>2</sub>, O<sub>2</sub><sup>-</sup>), Fe (III), Mn (II), SO<sub>2(aq)</sub>, and NO<sub>2(aq)</sub>. Considering the  
409 mutual influence of various factors in the reaction system can effectively prevent bias caused by  
410 arbitrarily fixing a certain value as was often done in previous studies.

## 411 **M. 3 Calculation of aerosol pH, aerosol liquid water, and ionic strength**

412 ALWC and aerosol pH were calculated using the ISORROPIA-II model and measured concentrations of  
413 inorganic ions in particles. ISORROPIA-II is a thermodynamic equilibrium model that predicts the  
414 physical state and composition of atmospheric inorganic aerosols. Its ability to predict pH has been  
415 demonstrated in detail in previous studies (Guo et al., 2015; Xu et al., 2015). Ionic strength was calculated  
416 via equation (2) (Ross and Noone, 1991):

$$417 \quad I_s = \frac{1}{2} \cdot \sum m_i \cdot z_i^2, \quad (2)$$

418 where  $m_i$  is the molality of an ion ( $\text{mol L}^{-1}$ ), and  $z_i$  is the corresponding charge. In the PKU-MARK  
419 model, reaction rates were replaced by the activity coefficient. The ionic strength was estimated using the  
420 ISORROPIA-II model assuming that the condensed phase is in the meta-stable state and complete  
421 external mixing state.

422 In order to consider the influence of particle diameter on aqueous  $\text{SO}_2$  concentrations, which is key to  
423 calculate sulfate formation, we used a 11-bin actual particle diameter distribution rather than one even  
424 distribution used in previous studies (Cheng et al., 2016). The distribution of particle number  
425 concentration and water content is illustrated in **Fig. S2**. We also considered the distribution of ALWC in  
426 different particle diameter bins based on the  $\kappa$ -Köhler theory (Petters and Kreidenweis, 2007) using  
427 observed kappa values from High Humidity Tandem Differential Mobility Analyser (HH-TDMA) and the  
428 Twin Differential Mobility Particle Sizer (TDMPS)/APS (Bian et al., 2014). Calculated ALWC values  
429 were strongly correlated with the ISORROPIA-II results (**Fig. S3**).

430 To combine both gas-phase molecular diffusion and liquid-phase interface mass transport processes, the  
431 approach adopted in this study uses one variable called  $k_{mt}$  (Schwartz, 1984; Schwartz, 1986), which is  
432 used in multiphase reactions in many modelling studies (Lelieveld and Crutzen, 1991; Chameides and  
433 Stelson, 1992b; Sander, 1999; Hanson et al., 1994). The definition of  $k_{mt}$  is given in equation (3):

$$434 \quad k_{mt} = \left( \frac{R_d^2}{3D_g} + \frac{4R_d}{3\nu_{\text{HO}_2}\alpha} \right)^{-1}. \quad (3)$$

435 The rate of gas-phase reactions ( $X$ ) diffusing and dissolving to the condensed phase can be calculated in  
436 the framework of aqueous-phase reactions as  $k_{mt,X} \times ALWC$  where  $X$  is the reactant molecule (please see  
437 **Table S8** for more details). Moreover, the conversion rate of aqueous-phase reactions to gas-phase  
438 reactions can be calculated as  $\frac{k_{mt,X}}{H^{cc} \times RT}$ . The unit of  $k_{mt}$  is  $\text{s}^{-1}$ , as  $k_{mt}$  contains the conversion from  $\text{m}_{\text{air}}^{-3}$  of  
439 the gas-phase molecule concentrations to  $\text{m}_{\text{aq}}^{-3}$  of the aqueous-phase molecule concentrations. Particle  
440 diameter can influence the mass transport rate of  $\text{SO}_2$  and its aqueous concentration. Based on the model  
441 results of (Xue et al., 2016), diameter had an impact on sulfate formation rates: for larger particles  
442 (radius  $>1 \mu\text{m}$ ),  $k_{mt}$  is determined by gas-phase diffusion; for smaller particles (radius  $<1 \mu\text{m}$ ),  $k_{mt}$  is

443 determined by the accommodation process. The PKU-MARK model can simultaneously simulate two-  
444 phase (gas and liquid) reaction systems in the same framework.

#### 445 **M. 4 Model Evaluation**

446 Concentrations of sulfate were calculated by integrating an extension of the Eulerian box model described  
447 in previous study (Seinfeld and Pandis, 2016). Sulfate concentrations are related to dry deposition,  
448 transport, dilution as the boundary layer height (BLH) expands, emissions, and net production. Due to the  
449 higher and more dramatically diurnal changing BLH in summer (Lou et al., 2019), and the lack of  
450 relevant data in WD-14 field campaign, we could not get the modelled results of sulfate concentrations in  
451 summer haze periods. Direct emissions and transport of sulfate were not considered in the calculation  
452 because secondary sulfate is the predominant source in winter haze periods. Dilution was not considered  
453 either because the atmosphere is relatively homogeneous during winter haze episodes. Since haze events  
454 are normally accompanied by a low boundary layer height ( $H_t$ ),  $H_t$  was set at 300 m at night-time and 450  
455 m at noon (Xue et al., 2016). At other times,  $H_t$  was estimated using a polynomial ( $n = 2$ ) regression as  
456 recommended in previous study (Xue et al., 2016). The diurnal trends of sulfate concentrations of the  
457 winter haze period using the deposition velocity of 1.5 cm/s and of 2 cm/s in summer are shown in **Fig. 1**  
458 **(c) and (d)**. Model results had the same trend with the observed values and could explain the missing  
459 source of sulfate aerosol to some extent in winter while with high uncertainties in summer condition.

460

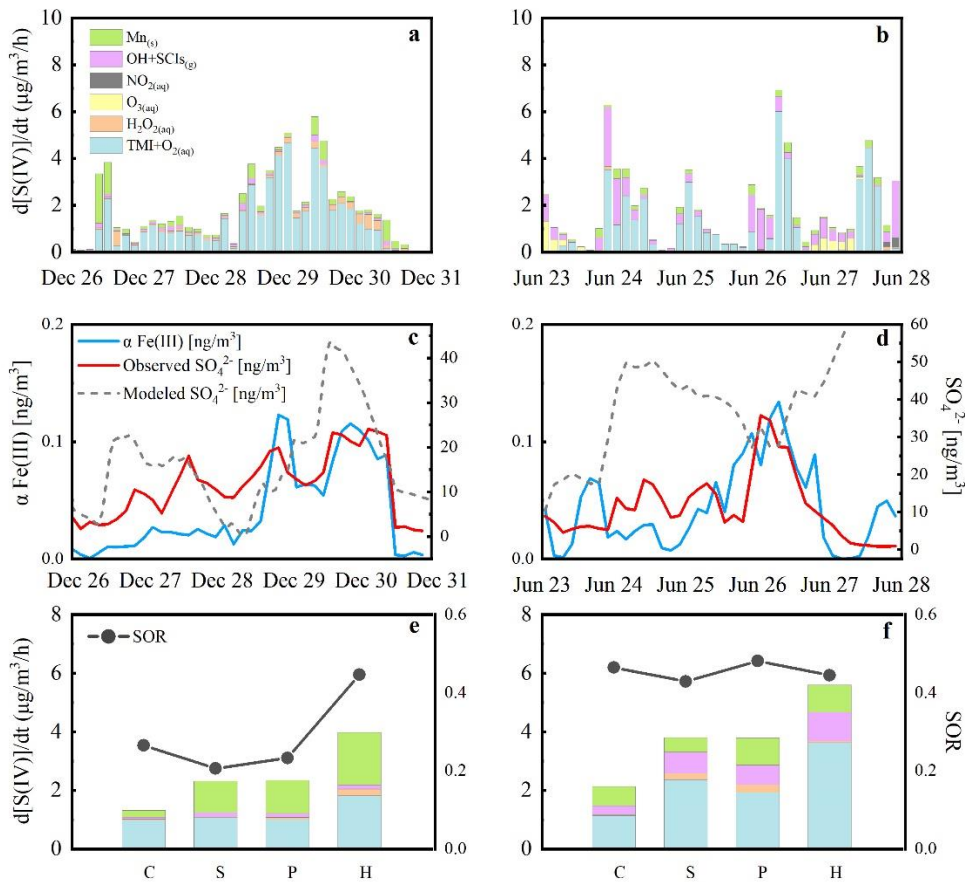
461

462 **Table 1. Averaged results of observed meteorological parameters, trace gases concentrations**  
 463 **transition metal concentrations such as Fe, Cu, Mn and calculated ALWC, ionic strength, pH and**  
 464 **sulfate formation rates in different pollution conditions in two field campaigns ( $\pm 1\sigma$ ).**

Parameters	Clean	Slightly polluted	Polluted	Highly polluted
<b>Winter</b>				
RH (%)	25.0 $\pm$ 8.3	37.1 $\pm$ 11.5	44.8 $\pm$ 11.9	63.6 $\pm$ 19.5
Temperature (K)	273.0 $\pm$ 4.6	274.1 $\pm$ 3.3	273.6 $\pm$ 2.6	273.8 $\pm$ 2.3
SO <sub>2</sub> (ppbV)	2.4 $\pm$ 1.4	5.8 $\pm$ 2.0	6.5 $\pm$ 2.6	5.5 $\pm$ 3.0
NO <sub>2</sub> (ppbV)	21.1 $\pm$ 10.4	37.6 $\pm$ 6.3	44.1 $\pm$ 6.1	57.6 $\pm$ 8.7
OH (#/cm <sup>3</sup> )	(4.67 $\pm$ 3.73) $\times 10^5$	(5.02 $\pm$ 5.22) $\times 10^5$	(4.42 $\pm$ 2.78) $\times 10^5$	(4.36 $\pm$ 3.06) $\times 10^5$
H <sub>2</sub> O <sub>2</sub> (pptV)	29.8 $\pm$ 20.8	23.5 $\pm$ 27.2	19.5 $\pm$ 39.6	20.9 $\pm$ 22.8
O <sub>3</sub> (ppbV)	14.8 $\pm$ 11.9	3.2 $\pm$ 5.7	2.1 $\pm$ 2.7	1.1 $\pm$ 1.2
SO <sub>4</sub> <sup>2-</sup> ( $\mu$ g/m <sup>3</sup> )	3.5 $\pm$ 1.5	6.4 $\pm$ 3.5	8.3 $\pm$ 4.2	16.6 $\pm$ 6.6
Fe (ng/m <sup>3</sup> )	348.4 $\pm$ 263.0	564.2 $\pm$ 188.2	725.5 $\pm$ 258.6	1300.6 $\pm$ 289.5
Cu (ng/m <sup>3</sup> )	7.0 $\pm$ 5.0	13.8 $\pm$ 4.2	18.7 $\pm$ 6.0	29.3 $\pm$ 6.6
Mn (ng/m <sup>3</sup> )	12.4 $\pm$ 9.4	20.1 $\pm$ 6.7	25.9 $\pm$ 9.2	46.5 $\pm$ 10.3
ALWC ( $\mu$ g/m <sup>3</sup> )	3.1 $\pm$ 2.6	3.8 $\pm$ 4.4	11.9 $\pm$ 15.6	82.4 $\pm$ 67.3
Surface area ( $\mu$ m <sup>2</sup> /cm <sup>3</sup> )	263.2 $\pm$ 171.5	714.3 $\pm$ 242.2	1253.3 $\pm$ 448.9	2628.6 $\pm$ 1164.4
PM <sub>2.5</sub> ( $\mu$ g/m <sup>3</sup> )	18.3 $\pm$ 10.1	52.0 $\pm$ 10.0	101.7 $\pm$ 18.2	190.0 $\pm$ 30.0
pH	4.43 $\pm$ 1.12	4.52 $\pm$ 0.76	4.93 $\pm$ 0.57	4.77 $\pm$ 0.39
Ionic Strength (M)	170.34 $\pm$ 88.32	89.32 $\pm$ 55.19	61.59 $\pm$ 38.7	36.27 $\pm$ 36.93
d[S(VI)]/dt ( $\mu$ g/m <sup>3</sup> /h)	1.3 $\pm$ 1.88	2.25 $\pm$ 2.15	2.35 $\pm$ 2.19	3.98 $\pm$ 2.75
<b>Summer</b>				
RH (%)	69.5 $\pm$ 17.9	64.4 $\pm$ 18.4	66.4 $\pm$ 13.0	65.6 $\pm$ 7.7
Temperature (K)	296.5 $\pm$ 3.6	298.5 $\pm$ 4.4	299.1 $\pm$ 2.9	298.9 $\pm$ 3.1

SO <sub>2</sub> (ppbV)	2.4±2.0	4.6±4.4	5.6±5.0	7.9±4.0
NO <sub>2</sub> (ppbV)	8.7±4.9	9.6±5.6	9.0±5.5	12.3±6.1
OH (#/cm <sup>3</sup> )	(2.38±2.44)×10 <sup>5</sup>	(3.27±3.21)×10 <sup>5</sup>	(2.77±2.26)×10 <sup>5</sup>	(3.50±3.38)×10 <sup>5</sup>
H <sub>2</sub> O <sub>2</sub> (pptV)	466.2±571.6	355.5±488.0	596.1±777.0	173.6±348.6
O <sub>3</sub> (ppbV)	46.0±30.3	50.9±30.6	53.0±26.6	48.5±28.5
SO <sub>2</sub> <sup>4-</sup> (μg/m <sup>3</sup> )	7.2±2.6	11.0±4.9	17.8±6.0	24.4±6.0
Fe (ng/m <sup>3</sup> )	521.6±286.6	469.3±151.7	535.2±177.0	730.9±156.6
Cu (ng/m <sup>3</sup> )	26.6±18.8	37.7±31.8	33.8±26.0	47.1±36.3
Mn (ng/m <sup>3</sup> )	18.6±10.2	16.8±5.4	19.1±6.3	26.1±5.6
ALWC (μg/m <sup>3</sup> )	31.8±30.9	35.7±32.8	48.6±31.4	58.8±14.4
Surface area (μm <sup>2</sup> /cm <sup>3</sup> )	767.8±265.6	925.0±213.9	1389.0±312.6	1711.1±729.6
PM <sub>2.5</sub> (μg/m <sup>3</sup> )	20.1±10.2	54.9±11.7	104.8±20.5	194.6±32.9
pH	4.48±0.48	4.19±0.66	4.17±0.48	4.33±0.44
Ionic Strength (M)	20.04±17.53	25.44±20.83	24.27±14.06	24.2±9.19
d[S(VI)]/dt (μg/m <sup>3</sup> /h)	2.13±2.03	3.81±4.22	3.79±5.66	5.6±4.45

465 The concentration of Mn was estimated based on the ratio of Fe/Mn observed in urban Beijing in the  
466 literatures (summarized in **Table S9**). All mentioned aerosol data is particle matters diameter smaller than  
467 2.5 μm, and PM<sub>2.5</sub> refers to the dry mass concentration of fine particulate matters.



468

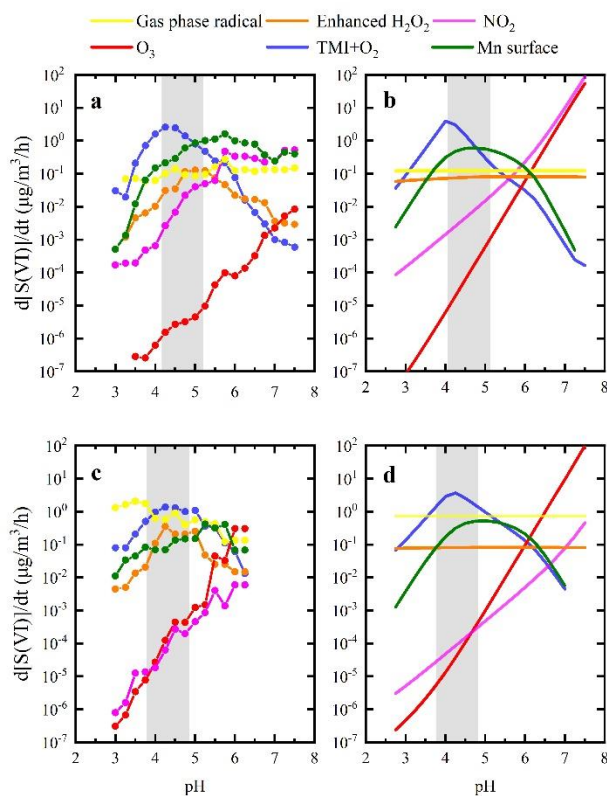
469 **Figure 1. Three-hour average sulfate formation rates during haze periods in winter and summer**  
 470 **(a)&(b), corresponding effective Fe (III) concentrations and sulfate concentrations (c)&(d), sulfate**  
 471 **formation rates (the histogram) and SOR (the dotted lines) in different pollution levels in two field**  
 472 **campaigns (e)&(f).**

473 The contributions to sulfate formation from each multiphase oxidant pathways including Mn-surface  
 474 oxidant (green), gas phase OH radical and Stabilized Criegee Intermediates (SCIs) oxidant (pink),  
 475 aqueous phase  $\text{NO}_2$  (grey),  $\text{O}_3$  (yellow),  $\text{H}_2\text{O}_2$  (orange) and aqTMI (blue) were coloured in the figure.  
 476 Obvious particle growth and removal was observed in winter (26<sup>th</sup> to 31<sup>st</sup>, December, 2017) and diurnal  
 477 variation patterns of sulfate concentration were observed in summer (23<sup>th</sup> to 28<sup>th</sup>, June, 2014). Diurnal  
 478 trends of modelled winter period's sulfate concentration (grey dash line) using deposition velocity as 1.5  
 479 cm/s in winter and 2 cm/s in summer are illustrated in panel (c) and (d). The dotted lines in the (e), winter

480 and (f), summer indicate the SOR with pollution level in the whole campaigns and the capitalized letters  
 481 “C”, “S”, “P”, “H” are the abbreviations for “Clean”, “Slightly polluted”, “Polluted” and “highly  
 482 polluted”, respectively.

483

484 **Figure 2. Multiphase sulfate production under actual ambient conditions (a, c) and averaged**  
 485 **conditions (b, d) in winter (a, b) and summer (c, d) in the North China Plain.**



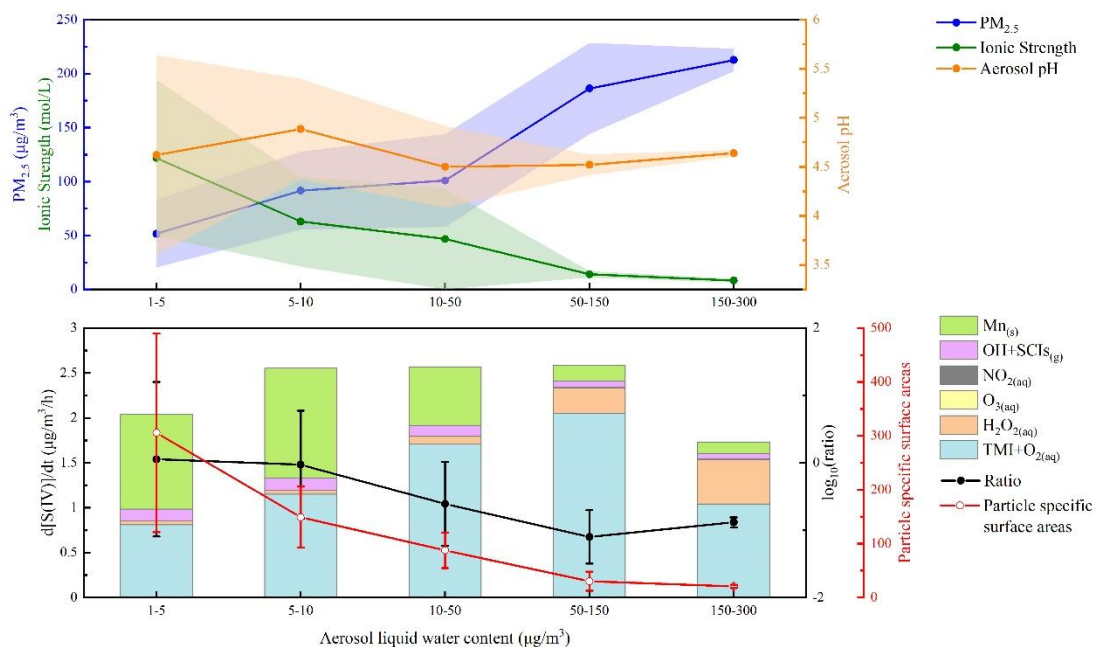
486

487 Given the actual measured concentration, the steady-state concentration of each reactant was calculated  
 488 using the MARK model accounting for the impact of ionic strength on the Henry’s law coefficient of the  
 489 gas-phase reactants. Panels (a) and (c) show the cluster averaged results with a pH span of 0.5. Panels (b)  
 490 and (d) show the sulfate formation rate obtained by fixing the average precursors levels during the haze  
 491 periods and by changing the aerosol pH, which is consistent with the calculation method of previous  
 492 studies (Cheng et al., 2016). Grey-shaded areas indicate the ISORROPIA-II (Fountoukis and Nenes,  
 493 2007) model calculated pH ranges during the haze periods of two field campaigns. The coloured solid



494 lines represent sulfate production rates calculated for different multiphase reaction pathways with  
 495 oxidants: enhanced  $\text{H}_2\text{O}_2$ ,  $\text{O}_3$ , TMIs,  $\text{NO}_2$ , surface Mn and gas-phase radicals ( $\text{OH}+\text{SCIs}$ ). The solid  
 496 orange line represents the calculated sulfate formation rate via  $\text{H}_2\text{O}_2$  with a factor of 100 in winter and  
 497 summer according to the latest research results (Liu et al., 2020b). Reactant concentrations, aqueous  
 498 reaction rate expressions, and rate coefficients are summarized in the SI.

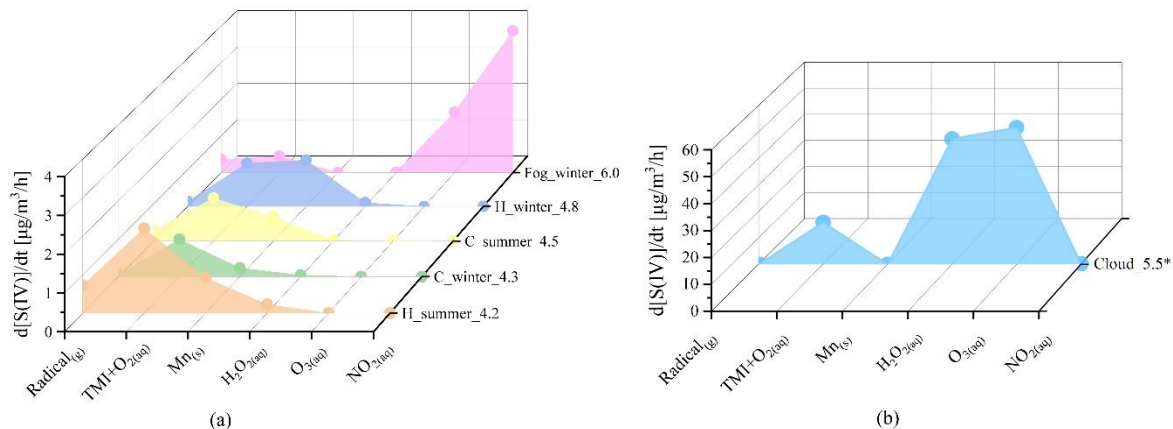
499 **Figure 3. Variation of  $\text{PM}_{2.5}$ , ionic strength, aerosol pH, particle specific surface areas and sulfate**  
 500 **formation rates from different pathways with aerosol liquid water content (ALWC) during winter**  
 501 **field campaign.**



502 The total number of valid data points shown in the figure is 479. The shaded area refers to the error bar  
 503 ( $\pm 1 \sigma$ ) of  $\text{PM}_{2.5}$  mass concentration, aerosol ionic strength and pH calculated by ISORROPIA-  
 504 II (Fountoukis and Nenes, 2007). Ratio in the second panel refers to the ratio of contributions from Mn-  
 505 surface to aqTMI to produce sulfate. Particle specific surface areas represent the ratio of particle surface  
 506 area ( $\mu\text{m}^2/\text{cm}^3$ ) and mass concentration ( $\mu\text{g}/\text{m}^3$ ).

507  
 508

509 **Figure 4. Bar graph showing modelled contributions of various pathways to sulfate formation**  
 510 **under different pollution conditions.**



511  
 512 Different pollution conditions including clear ( $\text{PM}_{2.5}$  smaller than  $35 \mu\text{g}/\text{m}^3$ ) in winter PKU 2017  
 513 (C\_winter\_4.3) and summer WD 2014 (C\_summer\_4.5); pollution ( $\text{PM}_{2.5}$  larger than  $75 \mu\text{g}/\text{m}^3$ ) in PKU  
 514 2017 (H\_winter\_4.8), WD 2014 (H\_summer\_4.2); fog conditions used in a previous study (Xue et al.,  
 515 2016) (Fog\_winter\_6.0) and cloud conditions (Cloud\_5.5) simulated by Seinfeld and Pandis (2016). The  
 516 number in each label indicates the average pH value chosen in these calculations. We assumed that the  
 517 cloud water content is  $0.1 \text{ g}/\text{m}^3$  in the last condition, and reduced the  $\text{H}_2\text{O}_2$  concentration to 0.1 ppb  
 518 compared to the high value used before (Seinfeld and Pandis, 2016).  
 519

## 520 **Data Availability**

521 Data supporting this publication are available upon request for the corresponding author

522 ([k.lu@pku.edu.cn](mailto:k.lu@pku.edu.cn)).

## 523 **Conflict of interests**

524 The authors declare that they have no conflict of interest.

## 525 **Acknowledgements**

526 This study was supported by the by the National Key Research and Development Program of China

527 (2019YFC0214800), the Beijing Municipal Natural Science Foundation for Distinguished Young

528 Scholars (JQ19031), the National Key Research Program for Air Pollution Control (DQGG202002), the

529 National Natural Science Foundation of China (21976006).

## 530 **Author Contributions**

531 Keding Lu conceived the study. Huan Song and Keding Lu developed the MARK model for multiphase

532 simulations. Can Ye provide supports in the calculation. Huan Song performed the model simulations and

533 wrote the manuscript with Keding Lu and Can Ye. Keding Lu and Yuanhang Zhang lead the two field

534 campaigns. Keding Lu, Huabin Dong, Shule Li, Shiyi Chen, Zhijun Wu, Mei Zheng, Limin Zeng, Min Hu

535 & Yuanhang Zhang provide campaign data for the analysis.

## 536 **Supplementary Information**

537

538 Supplementary information includes:

539 • Supplementary Information Text

540 Text S1. Activity coefficients of main reactants in the MARK model

541 Text S2. The concentration of aerosol particle transition metals in urban areas

542 • Supplementary Information Figures Fig.S1-S9

543 Fig. S1. Ionic strength of aerosol particle solution influence on the aqTMI rate constant.

544 Fig. S2. Distribution of ALWC and number concentration with aerosol particle bins in two  
545 campaigns.

546 Fig. S3. Calculated aerosol water by ISORROPIA-II model and H-TDMA method in two field  
547 campaigns during haze periods. The plots were coloured with the relative humidity values. The  
548 black dashed line in the figure is the 1:1 baseline, and the red solid line is the linear fitting result  
549 assuming the intercept is zero.

550 Fig. S4. Time series of observed gas-phase pollutants concentrations, RH, Temperature, PM2.5  
551 mass loading and calculated aerosol pH and water content and sulfate formation rates in these  
552 four haze periods in PKU-17 field campaign.

553 Fig. S5. SOR ( $\equiv n(\text{SO}_2)/n(\text{SO}_2+\text{SO}_4^{2-})$ ) correlations with effective Fe (III) concentrations in  
554 PKU-17 winter field campaign.

555 Fig. S6. SOR ( $\equiv n(\text{SO}_2)/n(\text{SO}_2+\text{SO}_4^{2-})$ ) correlations with odd oxygen ( $[\text{O}_x] \equiv [\text{O}_3]+[\text{NO}_2]$ ) and  
556 relative humidity (RH) in WD-14 summer field campaign

557 Fig. S7 the “dilution effect” of Fe mass concentration and ALWC increasing with PM mass in  
558 winter and summer.

559 Fig. S8. Variation of PM2.5, ionic strength, aerosol pH, particle specific surface areas and  
560 sulfate formation rates from different pathways with aerosol liquid water content (ALWC)  
561 during summer field campaign.

562 • Supplementary Information Tables S1-S9.

563 Table S1. Reaction rate expression and constant for SO<sub>2</sub> oxidation by OH in the gas-phase.

564 Table S2. Aqueous-phase reaction rate expressions, rate constants (k) and influence of ionic  
565 strength (Is) on k for sulfate production in aerosol particle condensed phase.

566 Table S3. Calculations of Henry’ law coefficients and influence of ionic strength.

567 Table S4. Typical activity coefficient values and expressions used in the MARK model.

568 Table S5. Kinetic data for the simulation of reactions in the aerosol particle condensed phase.

569	Table S6. Photolysis rates (aqueous phase) used in the model at noon ( $\text{sza} = 20^\circ$ )
570	Table S7. Aqueous equilibrium reactions
571	Table S8. Kinetic data for the simulation of gas-liquid phase conversion reactions
572	Table S9. Concentration of transition metals in PM <sub>2.5</sub> in urban areas.
573	• SI References
574	

## 575 **References**

- 576 Alexander, B., Park, R. J., Jacob, D. J., and Gong, S.: Transition metal-catalyzed oxidation of atmospheric sulfur:  
577 Global implications for the sulfur budget, *Journal of Geophysical Research: Atmospheres*, 114,  
578 <https://doi.org/10.1029/2008JD010486>, 2009.
- 579 Anttila, T., Kiendler-Scharr, A., Tillmann, R., and Mentel, T. F.: On the Reactive Uptake of Gaseous Compounds by  
580 Organic-Coated Aqueous Aerosols: Theoretical Analysis and Application to the Heterogeneous Hydrolysis of  
581 N<sub>2</sub>O<sub>5</sub>, *The Journal of Physical Chemistry A*, 110, 10435-10443, 10.1021/jp062403c, 2006.
- 582 Atkinson, R., Baulch, D. L., Cox, R. A., Crowley, J. N., Hampson, R. F., Hynes, R. G., Jenkin, M. E., Rossi, M. J.,  
583 and Troe, J.: Evaluated kinetic and photochemical data for atmospheric chemistry: Volume I - gas phase reactions of  
584 Ox, HOx, NOx and SOx species, *Atmospheric Chemistry and Physics*, 4, 1461-1738, 2004.
- 585 Baker, A. R. and Jickells, T. D.: Mineral particle size as a control on aerosol iron solubility, *Geophysical Research*  
586 *Letters*, 33, 10.1029/2006gl026557, 2006.
- 587 Baker, A. R., Jickells, T. D., Witt, M., and Linge, K. L.: Trends in the solubility of iron, aluminium, manganese and  
588 phosphorus in aerosol collected over the Atlantic Ocean, *Marine Chemistry*, 98, 43-58,  
589 10.1016/j.marchem.2005.06.004, 2006.
- 590 Barth, M. C., Hess, P. G., and Madronich, S.: Effect of marine boundary layer clouds on tropospheric chemistry as  
591 analyzed in a regional chemistry transport model, *Journal of Geophysical Research: Atmospheres*, 107, AAC 7-1-  
592 AAC 7-12, <https://doi.org/10.1029/2001JD000468>, 2002.
- 593 Bian, Y. X., Zhao, C. S., Ma, N., Chen, J., and Xu, W. Y.: A study of aerosol liquid water content based on  
594 hygroscopicity measurements at high relative humidity in the North China Plain, *Atmospheric Chemistry and*  
595 *Physics*, 14, 6417-6426, 10.5194/acp-14-6417-2014, 2014.
- 596 Chameides, W. and Stelson, A.: Aqueous - phase chemical processes in deliquescent sea - salt aerosols: A  
597 mechanism that couples the atmospheric cycles of S and sea salt, *Journal of Geophysical Research: Atmospheres*,  
598 97, 20565-20580, 1992a.
- 599 Chameides, W. L. and Stelson, A. W.: Aqueous-phase chemical processes in deliquescent seasalt aerosols, *Ber*  
600 *Bunsen Phys Chem*, 96, 461-470, 1992b.
- 601 Cheng, Y., Zheng, G., Wei, C., Mu, Q., Zheng, B., Wang, Z., Gao, M., Zhang, Q., He, K., Carmichael, G., Pöschl,  
602 U., and Su, H.: Reactive nitrogen chemistry in aerosol water as a source of sulfate during haze events in China,  
603 *Science Advances*, 2, e1601530, 10.1126/sciadv.1601530, 2016.
- 604 Duan, J. C., Tan, J. H., Wang, S. L., Hao, J. M., and Chail, F. H.: Size distributions and sources of elements in  
605 particulate matter at curbside, urban and rural sites in Beijing, *Journal of Environmental Sciences*, 24, 87-94,  
606 10.1016/s1001-0742(11)60731-6, 2012.
- 607 Fang, T., Guo, H., Zeng, L., Verma, V., Nenes, A., and Weber, R. J.: Highly Acidic Ambient Particles, Soluble  
608 Metals, and Oxidative Potential: A Link between Sulfate and Aerosol Toxicity, *Environ. Sci. Technol.*, 51, 2611-  
609 2620, 10.1021/acs.est.6b06151, 2017.
- 610 Folkers, M., Mentel, T. F., and Wahner, A.: Influence of an organic coating on the reactivity of aqueous aerosols  
611 probed by the heterogeneous hydrolysis of N<sub>2</sub>O<sub>5</sub>, *Geophysical Research Letters*, 30,  
612 <https://doi.org/10.1029/2003GL017168>, 2003.
- 613 Fountoukis, C. and Nenes, A.: ISORROPIA II: a computationally efficient thermodynamic equilibrium model for  
614 K<sup>+</sup>-Ca<sup>2+</sup>-Mg<sup>2+</sup>-NH<sub>4</sub><sup>+</sup>-Na<sup>+</sup>-SO<sub>4</sub><sup>2-</sup>-NO<sub>3</sub><sup>-</sup>-Cl<sup>-</sup>-H<sub>2</sub>O aerosols, *Atmospheric Chemistry and Physics Discussions*, 7, 1893-  
615 1939, 2007.
- 616 Gao, J., Peng, X., Chen, G., Xu, J., Shi, G.-L., Zhang, Y.-C., and Feng, Y.-C.: Insights into the chemical  
617 characterization and sources of PM<sub>2.5</sub> in Beijing at a 1-h time resolution, *Sci. Total Environ.*, 542, 162-171, 2016.
- 618 Gebel, M. E., Finlayson-Pitts, B. J., and Ganske, J. A.: The uptake of SO<sub>2</sub> on synthetic sea salt and some of its  
619 components, *Geophysical Research Letters*, 27, 887-890, <https://doi.org/10.1029/1999GL011152>, 2000.
- 620 Goliff, W. S. and Stockwell, W. R.: The regional atmospheric chemistry mechanism, version 2, an update,  
621 International conference on Atmospheric Chemical Mechanisms, University of California, Davis, 96, 36, 2008.
- 622 Goliff, W. S., Stockwell, W. R., and Lawson, C. V.: The regional atmospheric chemistry mechanism, version 2,  
623 *Atmos. Environ.*, 68, 174-185, 2013.
- 624 Guo, H., Weber, R. J., and Nenes, A.: High levels of ammonia do not raise fine particle pH sufficiently to yield  
625 nitrogen oxide-dominated sulfate production, *Sci Rep-Uk*, 7, 12109, 10.1038/s41598-017-11704-0, 2017.
- 626 Guo, H., Xu, L., Bougiatioti, A., Cerully, K. M., Capps, S. L., Hite, J. R., Carlton, A. G., Lee, S. H., Bergin, M. H.,  
627 Ng, N. L., Nenes, A., and Weber, R. J.: Fine-particle water and pH in the southeastern United States, *Atmospheric*  
628 *Chemistry and Physics*, 15, 5211-5228, 10.5194/acp-15-5211-2015, 2015.

629 Guo, S., Hu, M., Zamora, M. L., Peng, J. F., Shang, D. J., Zheng, J., Du, Z. F., Wu, Z., Shao, M., Zeng, L. M.,  
630 Molina, M. J., and Zhang, R. Y.: Elucidating severe urban haze formation in China, *Proceedings of the National*  
631 *Academy of Sciences of the United States of America*, 111, 17373-17378, 10.1073/pnas.1419604111, 2014.

632 Hanson, D. R., Ravishankara, A. R., and Solomon, S.: Heterogeneous reactions in sulfuric-acid aerosol: A  
633 framework for model calculations, *J. Geophys. Res.-Atmos.*, 99, 3615-3629, 10.1029/93jd02932, 1994.

634 He, P., Alexander, B., Geng, L., Chi, X., Fan, S., Zhan, H., Kang, H., Zheng, G., Cheng, Y., and Su, H.: Isotopic  
635 constraints on heterogeneous sulfate production in Beijing haze, *Atmospheric Chemistry and Physics*, 18, 5515-  
636 5528, 2018.

637 Heal, M. R., Hibbs, L. R., Agius, R. M., and Beverland, L. J.: Total and water-soluble trace metal content of urban  
638 background PM<sub>10</sub>, PM<sub>2.5</sub> and black smoke in Edinburgh, UK, *Atmos. Environ.*, 39, 1417-1430,  
639 10.1016/j.atmosphere.2004.11.026, 2005.

640 Hsu, S.-C., Wong, G. T. F., Gong, G.-C., Shiah, F.-K., Huang, Y.-T., Kao, S.-J., Tsai, F., Candice Lung, S.-C., Lin,  
641 F.-J., Lin, I. I., Hung, C.-C., and Tseng, C.-M.: Sources, solubility, and dry deposition of aerosol trace elements over  
642 the East China Sea, *Marine Chemistry*, 120, 116-127, <https://doi.org/10.1016/j.marchem.2008.10.003>, 2010.

643 Hu, W., Hu, M., Hu, W., Jimenez, J. L., Yuan, B., Chen, W., Wang, M., Wu, Y., Chen, C., Wang, Z., Peng, J., Zeng,  
644 L., and Shao, M.: Chemical composition, sources, and aging process of submicron aerosols in Beijing: Contrast  
645 between summer and winter, *Journal of Geophysical Research: Atmospheres*, 121, 1955-1977,  
646 <https://doi.org/10.1002/2015JD024020>, 2016.

647 Huang, K., Xia, S., Zhang, X.-M., Chen, Y.-L., Wu, Y.-T., and Hu, X.-B.: Comparative Study of the Solubilities of  
648 SO<sub>2</sub> in Five Low Volatile Organic Solvents (Sulfolane, Ethylene Glycol, Propylene Carbonate, N-Methylimidazole,  
649 and N-Methylpyrrolidone), *Journal of Chemical & Engineering Data*, 59, 1202-1212, 10.1021/je4007713, 2014a.

650 Huang, R.-J., Zhang, Y., Bozzetti, C., Ho, K.-F., Cao, J.-J., Han, Y., Daellenbach, K. R., Slowik, J. G., Platt, S. M.,  
651 Canonaco, F., Zotter, P., Wolf, R., Pieber, S. M., Bruns, E. A., Crippa, M., Ciarelli, G., Piazzalunga, A.,  
652 Schwikowski, M., Abbaszade, G., Schnelle-Kreis, J., Zimmermann, R., An, Z., Szidat, S., Baltensperger, U.,  
653 Haddad, I. E., and Prévôt, A. S. H.: High secondary aerosol contribution to particulate pollution during haze events  
654 in China, *Nature*, 514, 218-222, 10.1038/nature13774, 2014b.

655 Huang, X., Song, Y., Zhao, C., Li, M., Zhu, T., Zhang, Q., and Zhang, X.: Pathways of sulfate enhancement by  
656 natural and anthropogenic mineral aerosols in China, *Journal of Geophysical Research: Atmospheres*, 119, 14,165-  
657 114,179, <https://doi.org/10.1002/2014JD022301>, 2014c.

658 Ito, A., Myriokefalitakis, S., Kanakidou, M., Mahowald, N. M., Scanza, R. A., Hamilton, D. S., Baker, A. R.,  
659 Jickells, T., Sarin, M., Bikina, S., Gao, Y., Shelley, R. U., Buck, C. S., Landing, W. M., Bowie, A. R., Perron, M.  
660 M. G., Guieu, C., Meskhidze, N., Johnson, M. S., Feng, Y., Kok, J. F., Nenes, A., and Duce, R. A.: Pyrogenic iron:  
661 The missing link to high iron solubility in aerosols, *Science Advances*, 5, eaau7671, 10.1126/sciadv.aau7671, 2019.

662 Koop, T., Luo, B., Tsias, A., and Peter, T.: Water activity as the determinant for homogeneous ice nucleation in  
663 aqueous solutions, *Nature*, 406, 611-614, 2000.

664 Lelieveld, J. and Crutzen, P. J.: The role of clouds in tropospheric photochemistry, *J Atmos Chem*, 12, 229-267,  
665 10.1007/bf00048075, 1991.

666 Li, J., Zhang, Y.-L., Cao, F., Zhang, W., Fan, M., Lee, X., and Michalski, G.: Stable Sulfur Isotopes Revealed a  
667 Major Role of Transition-Metal Ion-Catalyzed SO<sub>2</sub> Oxidation in Haze Episodes, *Environ. Sci. Technol.*, 54, 2626-  
668 2634, 10.1021/acs.est.9b07150, 2020a.

669 Li, J., Zhu, C., Chen, H., Fu, H., Xiao, H., Wang, X., Herrmann, H., and Chen, J.: A More Important Role for the  
670 Ozone-S(IV) Oxidation Pathway Due to Decreasing Acidity in Clouds, *Journal of Geophysical Research:*  
671 *Atmospheres*, 125, e2020JD033220, <https://doi.org/10.1029/2020JD033220>, 2020b.

672 Li, L., Hoffmann, M. R., and Colussi, A. J.: Role of Nitrogen Dioxide in the Production of Sulfate during Chinese  
673 Haze-Aerosol Episodes, *Environ. Sci. Technol.*, 52, 2686-2693, 10.1021/acs.est.7b05222, 2018.

674 Lippmann, M. and Thurston, G. D.: Sulfate concentrations as an indicator of ambient particulate matter air pollution  
675 for health risk evaluations, *J Expo Anal Environ Epidemiol*, 6, 123-146, 1996.

676 Liu, C., Ma, Q., Liu, Y., Ma, J., and He, H.: Synergistic reaction between SO<sub>2</sub> and NO<sub>2</sub> on mineral oxides: a  
677 potential formation pathway of sulfate aerosol, *Physical Chemistry Chemical Physics*, 14, 1668-1676,  
678 10.1039/C1CP22217A, 2012.

679 Liu, J., Chen, Y., Chao, S., Cao, H., Zhang, A., and Yang, Y.: Emission control priority of PM<sub>2.5</sub>-bound heavy  
680 metals in different seasons: A comprehensive analysis from health risk perspective, *Sci. Total Environ.*, 644, 20-30,  
681 <https://doi.org/10.1016/j.scitotenv.2018.06.226>, 2018.

682 Liu, M., Song, Y., Zhou, T., Xu, Z., Yan, C., Zheng, M., Wu, Z., Hu, M., Wu, Y., and Zhu, T.: Fine particle pH  
683 during severe haze episodes in northern China, *Geophysical Research Letters*, 44, 5213-5221,  
684 <https://doi.org/10.1002/2017GL073210>, 2017.

685 Liu, P., Ye, C., Xue, C., Zhang, C., Mu, Y., and Sun, X.: Formation mechanisms of atmospheric nitrate and sulfate  
686 during the winter haze pollution periods in Beijing: gas-phase, heterogeneous and aqueous-phase chemistry,  
687 *Atmospheric Chemistry and Physics*, 20, 4153-4165, 2020a.

688 Liu, T., Clegg, S. L., and Abbatt, J. P. D.: Fast oxidation of sulfur dioxide by hydrogen peroxide in deliquesced  
689 aerosol particles, *Proceedings of the National Academy of Sciences*, 117, 1354-1359, 10.1073/pnas.1916401117,  
690 2020b.

691 Lou, M., Guo, J., Wang, L., Xu, H., Chen, D., Miao, Y., Lv, Y., Li, Y., Guo, X., Ma, S., and Li, J.: On the  
692 Relationship Between Aerosol and Boundary Layer Height in Summer in China Under Different Thermodynamic  
693 Conditions, *Earth and Space Science*, 6, 887-901, <https://doi.org/10.1029/2019EA000620>, 2019.

694 Ma, T., Furutani, H., Duan, F., Kimoto, T., Jiang, J., Zhang, Q., Xu, X., Wang, Y., Gao, J., Geng, G., Li, M., Song,  
695 S., Ma, Y., Che, F., Wang, J., Zhu, L., Huang, T., Toyoda, M., and He, K.: Contribution of  
696 hydroxymethanesulfonate (HMS) to severe winter haze in the North China Plain, *Atmos. Chem. Phys.*, 20, 5887-  
697 5897, 10.5194/acp-20-5887-2020, 2020.

698 Ma, X., Tan, Z., Lu, K., Yang, X., Liu, Y., Li, S., Li, X., Chen, S., Novelli, A., and Cho, C.: Winter photochemistry  
699 in Beijing: Observation and model simulation of OH and HO<sub>2</sub> radicals at an urban site, *Sci. Total Environ.*, 685, 85-  
700 95, 2019.

701 Mahowald, N. M., Baker, A. R., Bergametti, G., Brooks, N., Duce, R. A., Jickells, T. D., Kubilay, N., Prospero, J.  
702 M., and Tegen, I.: Atmospheric global dust cycle and iron inputs to the ocean, *Global Biogeochemical Cycles*, 19,  
703 <https://doi.org/10.1029/2004GB002402>, 2005.

704 Moch, J. M., Dovrou, E., Mickley, L. J., Keutsch, F. N., Cheng, Y., Jacob, D. J., Jiang, J., Li, M., Munger, J. W.,  
705 and Qiao, X.: Contribution of hydroxymethane sulfonate to ambient particulate matter: A potential explanation for  
706 high particulate sulfur during severe winter haze in Beijing, *Geophysical Research Letters*, 45, 11,969-911,979,  
707 2018.

708 Oakes, M., Rastogi, N., Majestic, B. J., Shafer, M., Schauer, J. J., Edgerton, E. S., and Weber, R. J.: Characterization  
709 of soluble iron in urban aerosols using near-real time data, *Journal of Geophysical Research: Atmospheres*, 115,  
710 <https://doi.org/10.1029/2009JD012532>, 2010.

711 Petters, M. D. and Kreidenweis, S. M.: A single parameter representation of hygroscopic growth and cloud  
712 condensation nucleus activity, *Atmos. Chem. Phys.*, 7, 1961-1971, 10.5194/acp-7-1961-2007, 2007.

713 Ross, H. B. and Noone, K. J.: A numerical investigation of the destruction of peroxy radical by cu ion catalyzed-  
714 reactions on atmospheric particles, *J Atmos Chem*, 12, 121-136, 10.1007/bf00115775, 1991.

715 Ryder, O. S., Campbell, N. R., Morris, H., Forestieri, S., Ruppel, M. J., Cappa, C., Tivanski, A., Prather, K., and  
716 Bertram, T. H.: Role of Organic Coatings in Regulating N<sub>2</sub>O<sub>5</sub> Reactive Uptake to Sea Spray Aerosol, *The Journal*  
717 *of Physical Chemistry A*, 119, 11683-11692, 10.1021/acs.jpca.5b08892, 2015.

718 Sander, R.: Modeling atmospheric chemistry: Interactions between gas-phase species and liquid cloud/aerosol  
719 particles, *Surveys in Geophysics*, 20, 1-31, 1999.

720 Sarwar, G., J. Godowitch, K. Fahey, J. Xing, David-C Wong, Jeff Young, S. Roselle, AND R. Mathur: Examination  
721 of Sulfate production by CB05TU, RACM2 & RACM2 with SCI initiated SO<sub>2</sub> oxidation in the Northern  
722 Hemisphere, Presented at Presentation at the CMAS Conference, Chapel Hill, NC2013.

723 Schwartz, S. E.: Gas phase and aqueous phase chemistry of HO<sub>2</sub> in liquid water clouds, *J. Geophys. Res.-Atmos.*,  
724 89, 1589-1598, 10.1029/JD089iD07p11589, 1984.

725 Schwartz, S. E.: Mass-transport considerations pertinent to aqueous phase reactions of gases in liquid-water clouds,  
726 in: *Chemistry of multiphase atmospheric systems*, Springer, 415-471, 1986.

727 Seigneur, C. and Saxena, P.: A theoretical investigation of sulfate formation in clouds, *Atmospheric Environment*  
728 (1967), 22, 101-115, [https://doi.org/10.1016/0004-6981\(88\)90303-4](https://doi.org/10.1016/0004-6981(88)90303-4), 1988.

729 Seinfeld, J. H. and Pandis, S. N.: *Atmospheric chemistry and physics: from air pollution to climate change*, John  
730 Wiley & Sons2016.

731 Shang, D., Peng, J., Guo, S., Wu, Z., and Hu, M.: Secondary aerosol formation in winter haze over the Beijing-  
732 Tianjin-Hebei Region, China, *Frontiers of Environmental Science & Engineering*, 15, 34, 10.1007/s11783-020-  
733 1326-x, 2020.

734 Shao, J., Chen, Q., Wang, Y., Lu, X., He, P., Sun, Y., Shah, V., Martin, R. V., Philip, S., Song, S., Zhao, Y., Xie, Z.,  
735 Zhang, L., and Alexander, B.: Heterogeneous sulfate aerosol formation mechanisms during wintertime Chinese haze  
736 events: air quality model assessment using observations of sulfate oxygen isotopes in Beijing, *Atmos. Chem. Phys.*,  
737 19, 6107-6123, 10.5194/acp-19-6107-2019, 2019.

738 Shi, Q., Tao, Y., Krechmer, J. E., Heald, C. L., Murphy, J. G., Kroll, J. H., and Ye, Q.: Laboratory Investigation of  
739 Renoxification from the Photolysis of Inorganic Particulate Nitrate, *Environ. Sci. Technol.*, 55, 854-861,  
740 10.1021/acs.est.0c06049, 2021.



741 Shi, Z., Krom, M. D., Jickells, T. D., Bonneville, S., Carslaw, K. S., Mihalopoulos, N., Baker, A. R., and Benning,  
742 L. G.: Impacts on iron solubility in the mineral dust by processes in the source region and the atmosphere: A review,  
743 *Aeolian Research*, 5, 21-42, <https://doi.org/10.1016/j.aeolia.2012.03.001>, 2012.

744 Sholkovitz, E. R., Sedwick, P. N., Church, T. M., Baker, A. R., and Powell, C. F.: Fractional solubility of aerosol  
745 iron: Synthesis of a global-scale data set, *Geochimica et Cosmochimica Acta*, 89, 173-189,  
746 <https://doi.org/10.1016/j.gca.2012.04.022>, 2012.

747 Song, H., Chen, X., Lu, K., Zou, Q., Tan, Z., Fuchs, H., Wiedensohler, A., Zheng, M., Wahner, A., Kiendler-Scharr,  
748 A., and Zhang, Y.: Influence of aerosol copper on HO<sub>2</sub> uptake: A novel parameterized equation, *Atmos. Chem.*  
749 *Phys. Discuss.*, 2020, 1-23, 10.5194/acp-2020-218, 2020.

750 Tan, Z. F., Fuchs, H., Lu, K. D., Hofzumahaus, A., Bohn, B., Broch, S., Dong, H. B., Gomm, S., Haseler, R., He, L.  
751 Y., Holland, F., Li, X., Liu, Y., Lu, S. H., Rohrer, F., Shao, M., Wang, B. L., Wang, M., Wu, Y. S., Zeng, L. M.,  
752 Zhang, Y. S., Wahner, A., and Zhang, Y. H.: Radical chemistry at a rural site (Wangdu) in the North China Plain:  
753 observation and model calculations of OH, HO<sub>2</sub> and RO<sub>2</sub> radicals, *Atmospheric Chemistry and Physics*, 17, 663-  
754 690, 10.5194/acp-17-663-2017, 2017.

755 Wang, G., Zhang, R., Gomez, M. E., Yang, L., Zamora, M. L., Hu, M., Lin, Y., Peng, J., Guo, S., Meng, J., Li, J.,  
756 Cheng, C., Hu, T., Ren, Y., Wang, Y., Gao, J., Cao, J., An, Z., Zhou, W., Li, G., Wang, J., Tian, P., Marrero-Ortiz,  
757 W., Secret, J., Du, Z., Zheng, J., Shang, D., Zeng, L., Shao, M., Wang, W., Huang, Y., Wang, Y., Zhu, Y., Li, Y.,  
758 Hu, J., Pan, B., Cai, L., Cheng, Y., Ji, Y., Zhang, F., Rosenfeld, D., Liss, P. S., Duce, R. A., Kolb, C. E., and Molina,  
759 M. J.: Persistent sulfate formation from London Fog to Chinese haze, *Proceedings of the National Academy of*  
760 *Sciences of the United States of America*, 113, 13630-13635, 10.1073/pnas.1616540113, 2016.

761 Wang, W., Liu, M., Wang, T., Song, Y., Zhou, L., Cao, J., Hu, J., Tang, G., Chen, Z., Li, Z., Xu, Z., Peng, C., Lian,  
762 C., Chen, Y., Pan, Y., Zhang, Y., Sun, Y., Li, W., Zhu, T., Tian, H., and Ge, M.: Sulfate formation is dominated by  
763 manganese-catalyzed oxidation of SO<sub>2</sub> on aerosol surfaces during haze events, *Nature Communications*, 12, 1993,  
764 10.1038/s41467-021-22091-6, 2021.

765 Wang, X., Gemayel, R., Hayeck, N., Perrier, S., Charbonnel, N., Xu, C., Chen, H., Zhu, C., Zhang, L., Wang, L.,  
766 Nizkorodov, S. A., Wang, X., Wang, Z., Wang, T., Mellouki, A., Riva, M., Chen, J., and George, C.: Atmospheric  
767 Photosensitization: A New Pathway for Sulfate Formation, *Environ. Sci. Technol.*, 54, 3114-3120,  
768 10.1021/acs.est.9b06347, 2020.

769 Weber, R. J., Guo, H., Russell, A. G., and Nenes, A.: High aerosol acidity despite declining atmospheric sulfate  
770 concentrations over the past 15 years, *Nature Geoscience*, 9, 282-285, 10.1038/ngeo2665, 2016.

771 Welz, O., Savee, J. D., Osborn, D. L., Vasu, S. S., Percival, C. J., Shallcross, D. E., and Taatjes, C. A.: Direct  
772 Kinetic Measurements of Criegee Intermediate (CH<sub>2</sub>OO) Formed by Reaction of CH<sub>2</sub>I with O<sub>2</sub><sup>-</sup>, *Science*, 335, 204-  
773 207, 10.1126/science.1213229, 2012.

774 Wong, J. P. S., Yang, Y., Fang, T., Mulholland, J. A., Russell, A. G., Ebel, S., Nenes, A., and Weber, R. J.: Fine  
775 Particle Iron in Soils and Road Dust Is Modulated by Coal-Fired Power Plant Sulfur, *Environ. Sci. Technol.*, 54,  
776 7088-7096, 10.1021/acs.est.0c00483, 2020.

777 Xu, L., Guo, H., Boyd, C. M., Klein, M., Bougiatioti, A., Cerully, K. M., Hite, J. R., Isaacman-VanWertz, G.,  
778 Kreisberg, N. M., and Knute, C.: Effects of anthropogenic emissions on aerosol formation from isoprene and  
779 monoterpenes in the southeastern United States, *Proceedings of the National Academy of Sciences*, 112, 37-42,  
780 2015.

781 Xue, J., Yuan, Z., Griffith, S. M., Yu, X., Lau, A. K. H., and Yu, J. Z.: Sulfate Formation Enhanced by a Cocktail of  
782 High NO<sub>x</sub>, SO<sub>2</sub>, Particulate Matter, and Droplet pH during Haze-Fog Events in Megacities in China: An  
783 Observation-Based Modeling Investigation, *Environ. Sci. Technol.*, 50, 7325-7334, 10.1021/acs.est.6b00768, 2016.

784 Yao, M., Zhao, Y., Hu, M. H., Huang, D. D., Wang, Y. C., Yu, J. Z., and Yan, N. Q.: Multiphase Reactions between  
785 Secondary Organic Aerosol and Sulfur Dioxide: Kinetics and Contributions to Sulfate Formation and Aerosol  
786 Aging, *Environmental Science & Technology Letters*, 6, 768-774, 10.1021/acs.estlett.9b00657, 2019.

787 Ye, C., Liu, P., Ma, Z., Xue, C., Zhang, C., Zhang, Y., Liu, J., Liu, C., Sun, X., and Mu, Y.: High H<sub>2</sub>O<sub>2</sub>  
788 Concentrations Observed during Haze Periods during the Winter in Beijing: Importance of H<sub>2</sub>O<sub>2</sub> Oxidation in  
789 Sulfate Formation, *Environmental Science & Technology Letters*, 5, 757-763, 10.1021/acs.estlett.8b00579, 2018.

790 Young, L.-H., Li, C.-H., Lin, M.-Y., Hwang, B.-F., Hsu, H.-T., Chen, Y.-C., Jung, C.-R., Chen, K.-C., Cheng, D.-  
791 H., and Wang, V.-S.: Field performance of a semi-continuous monitor for ambient PM<sub>2.5</sub> water-soluble inorganic  
792 ions and gases at a suburban site, *Atmos. Environ.*, 144, 376-388, 2016.

793 Yu, H., Li, W., Zhang, Y., Tunved, P., Dall'Osto, M., Shen, X., Sun, J., Zhang, X., Zhang, J., and Shi, Z.: Organic  
794 coating on sulfate and soot particles during late summer in the Svalbard Archipelago, *Atmos. Chem. Phys.*, 19,  
795 10433-10446, 10.5194/acp-19-10433-2019, 2019.

796 Yue, F., He, P., Chi, X., Wang, L., Yu, X., Zhang, P., and Xie, Z.: Characteristics and major influencing factors of  
797 sulfate production via heterogeneous transition-metal-catalyzed oxidation during haze evolution in China, *Atmos.*  
798 *Pollut. Res.*, 11, 1351-1358, <https://doi.org/10.1016/j.apr.2020.05.014>, 2020.

799 Zelenov, V. V., Aparina, E. V., Kashtanov, S. A., and Shardakova, E. V.: Kinetics of NO<sub>3</sub> uptake on a methane soot  
800 coating, *Russian Journal of Physical Chemistry B*, 11, 180-188, 10.1134/s1990793117010146, 2017.

801 Zhang, B., Zhou, T., Liu, Y., Yan, C., Li, X., Yu, J., Wang, S., Liu, B., and Zheng, M.: Comparison of water-soluble  
802 inorganic ions and trace metals in PM<sub>2.5</sub> between online and offline measurements in Beijing during winter, *Atmos.*  
803 *Pollut. Res.*, 10, 1755-1765, <https://doi.org/10.1016/j.apr.2019.07.007>, 2019.

804 Zhang, N., Zhang, J., Zhang, Y., Bai, J., and Wei, X.: Solubility and Henry's law constant of sulfur dioxide in  
805 aqueous polyethylene glycol 300 solution at different temperatures and pressures, *Fluid Phase Equilibria*, 348, 9-16,  
806 <https://doi.org/10.1016/j.fluid.2013.03.006>, 2013.

807 Zhang, X., Zhuang, G., Chen, J., Wang, Y., Wang, X., An, Z., and Zhang, P.: Heterogeneous Reactions of Sulfur  
808 Dioxide on Typical Mineral Particles, *The Journal of Physical Chemistry B*, 110, 12588-12596, 10.1021/jp0617773,  
809 2006.

810 Zhao, D., Song, X., Zhu, T., Zhang, Z., Liu, Y., and Shang, J.: Multiphase oxidation of SO<sub>2</sub> by NO<sub>2</sub> on CaCO<sub>3</sub>  
811 particles, *Atmos. Chem. Phys.*, 18, 2481-2493, 10.5194/acp-18-2481-2018, 2018.

812 Zhao, S., Tian, H., Luo, L., Liu, H., Wu, B., Liu, S., Bai, X., Liu, W., Liu, X., Wu, Y., Lin, S., Guo, Z., Lv, Y., and  
813 Xue, Y.: Temporal variation characteristics and source apportionment of metal elements in PM<sub>2.5</sub> in urban Beijing  
814 during 2018 - 2019, *Environ. Pollut.*, 268, 115856, <https://doi.org/10.1016/j.envpol.2020.115856>, 2021.

815 Zheng, B., Zhang, Q., Zhang, Y., He, K. B., Wang, K., Zheng, G. J., Duan, F. K., Ma, Y. L., and Kimoto, T.:  
816 Heterogeneous chemistry: a mechanism missing in current models to explain secondary inorganic aerosol formation  
817 during the January 2013 haze episode in North China, *Atmos. Chem. Phys.*, 15, 2031-2049, 10.5194/acp-15-2031-  
818 2015, 2015.

819 Zheng, H., Song, S., Sarwar, G., Gen, M., Wang, S., Ding, D., Chang, X., Zhang, S., Xing, J., Sun, Y., Ji, D., Chan,  
820 C. K., Gao, J., and McElroy, M. B.: Contribution of Particulate Nitrate Photolysis to Heterogeneous Sulfate  
821 Formation for Winter Haze in China, *Environmental Science & Technology Letters*, 7, 632-638,  
822 10.1021/acs.estlett.0c00368, 2020.

823 Zhu, Y., Tilgner, A., Hoffmann, E. H., Herrmann, H., Kawamura, K., Yang, L., Xue, L., and Wang, W.: Multiphase  
824 MCM-CAPRAM modeling of the formation and processing of secondary aerosol constituents observed during the  
825 Mt. Tai summer campaign in 2014, *Atmospheric Chemistry and Physics*, 20, 6725-6747, 2020a.

826 Zhu, Y., Li, W., Lin, Q., Yuan, Q., Liu, L., Zhang, J., Zhang, Y., Shao, L., Niu, H., Yang, S., and Shi, Z.: Iron  
827 solubility in fine particles associated with secondary acidic aerosols in east China, *Environ. Pollut.*, 264, 114769,  
828 <https://doi.org/10.1016/j.envpol.2020.114769>, 2020b.

829